On the formation of glass microelectrodes

HUANG, Huaxiong; WYLIE, Jonathan J.; MIURA, Robert M.; HOWELL, Peter D.

Published in:
SIAM Journal on Applied Mathematics

Published: 01/01/2007

Document Version:
Final Published version, also known as Publisher's PDF, Publisher's Final version or Version of Record

Published version (DOI):
10.1137/050640722

Publication details:
HUANG, H., WYLIE, J. J., MIURA, R. M., & HOWELL, P. D. (2007). On the formation of glass microelectrodes. *SIAM Journal on Applied Mathematics*, *67*(3), 630-666. https://doi.org/10.1137/050640722

SIAM J. APPL. MATH.
Vol. 67, No. 3, pp. 630–666

ON THE FORMATION OF GLASS MICROELECTRODES*

HUAXIONG HUANG†, JONATHAN J. WYLIE‡, ROBERT M. MIURA§, AND PETER D. HOWELL¶

Abstract. Glass microelectrodes are used widely in experimental studies of the electrophysiology of biological cells and their membranes. However, the pulling of these electrodes remains an art, based on trial and error. Following Huang et al. [*SIAM J. Appl. Math.*, 63 (2003), pp. 1499–1519], we derive a one-dimensional model for the stretching of a hollow glass tube that is being radiatively heated. Our framework allows us to consider two commonly used puller designs, that is, horizontal (constant force) and vertical (variable force) pullers. We derive explicit solutions and use these solutions to identify the principal factors that control the final shape of the microelectrodes. The design implications for pullers also are discussed.

Key words. free-boundary problem, glass microelectrode, heat transfer, incompressible fluids, long-wave approximation, partial differential equations, temperature-dependent viscosity

AMS subject classifications. 76D27, 80A20, 35L60

DOI. 10.1137/050640722

1. Introduction.

Glass microelectrodes have played an essential role in cell electrophysiology for decades and will continue to be an important tool in the future. These micropipettes are used to measure membrane potentials and inject electric current and dyes into cells. This is done by inserting the electrode tips through cellular membranes or by "patching" the electrode tip to the membrane. The data collected by these techniques provide crucial information about the electrical properties of the membrane, e.g., the voltage-gated and receptor-gated ion channels, under various conditions, including during drug applications. Laboratories generally produce these microelectrodes on a daily basis using commercially available glass tubes and mechanical microelectrode pullers. For more descriptions of the medical applications of these electrodes, we refer interested readers to [16, 15], and references therein.

Electrode pullers vary in design, but all have the same basic features. They start with a uniform glass tube and heat a small section using a radiative heating element. As the glass is heated, a pulling force is applied along the axis of the tube. When the glass temperature becomes sufficiently high, its viscosity decreases dramatically, and the glass tube stretches rapidly. The tube then becomes extremely thin, ultimately breaks, and each half of the tube can be used as an electrode. Pullers are designed to

*Received by the editors September 19, 2005; accepted for publication (in revised form) October 17, 2006; published electronically February 26, 2007.
http://www.siam.org/journals/siap/67-3/64072.html

†School of Mathematics, Fudan University, Shanghai, China 200433, and Department of Mathematics and Statistics, York University, Toronto, Ontario M3J 1P3, Canada (hhuang@yorku.ca). This author's research was supported in part by grants from the Natural Sciences and Engineering Research Council of Canada and the Mathematics of Information Technology and Complex Systems of Canada.

‡Department of Mathematics, City University of Hong Kong, Kowloon, Hong Kong (mawylie@cityu.edu.hk). This author's work was supported by a grant from the City University of Hong Kong (projects 7001560 and 7001714).

§Department of Mathematical Sciences, New Jersey Institute of Technology, Newark, NJ 07102 (miura@njit.edu). This author's research was supported by the Department of Mathematical Sciences, New Jersey Institute of Technology.

¶Oxford Centre for Industrial and Applied Mathematics, Mathematical Institute, University of Oxford, Oxford OX1 3LB, UK (howell@maths.ox.ac.uk).

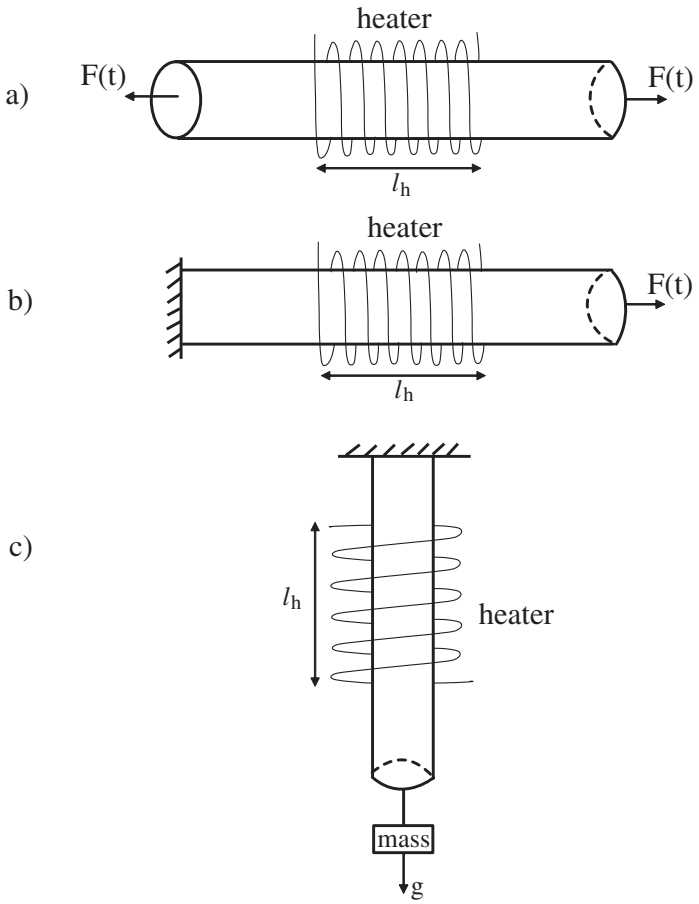

FIG. 1.1. *Three possible pullers.* (a) *Horizontal puller with free-moving ends and equal forces.* (b) *Horizontal puller with one fixed end and a single force.* (c) *Vertical puller with mass under gravity.*

achieve this result in different ways. For example, the pulling force may be achieved using electromagnets or by simply attaching a weight to one end of the tube. Electrodes may be formed in a single pull, or the glass can be stretched, allowed to cool, and subjected to a second pull that then breaks the tube. Designs for three possible pullers are shown in Figure 1.1.

Glass microelectrodes can be characterized by four experimentally relevant parameters. These are the tip length, tip diameter, electrode resistance, and electrode capacitance. Tip length is significant because it determines the physical strength of the electrode and the ease with which it can penetrate tissue and cells. A short steeply tapered tip is robust but does not penetrate tissue easily. The converse is true of long gently tapered tips. The tip shape also affects its electrical resistance and capacitance. More information on the relevance of the tip shape to physical parameters can be found in [8] and [18].

During the actual manufacturing process, the exact relationship between the variables (heater geometry, rate of pulling the glass tube, length of first pull (for a patch electrode), rate of the second pull, etc.) and electrode properties is usually determined empirically by trial and error. Although some work has been done towards

understanding how the final electrode shape is influenced by the heater geometry and width [8], in general the process is not well determined. In a previous paper [12], we developed a basic mathematical model for the formation process of these glass microelectrodes and, through computer simulations, showed that the model was capable of predicting, relatively closely, the breakup process observed in the laboratory.

The results in [12] illustrate several features that are fundamental in understanding the pulling process. First, the glass tube initially stretches very little due to the large value of the viscosity at room temperature. As the portion of the tube that is being heated by the heating element increases in temperature, the viscosity of the glass tube decreases dramatically, and the extension and breakup of the glass tube occur very rapidly. During this time, the temperature of the glass tube locally remains approximately constant; i.e., the effects of thermal diffusion and radiation are negligible.

In this paper, we derive a simplified model that captures the principal physics underlying the electrode formation. Using a dimensional analysis argument, we show that the conductive heat transfer is small compared to the radiative and convective heat transfer, and therefore conduction can be neglected in the temperature equation. We develop a general method to solve the model equations and, in some special cases, compute explicit solutions to the time-dependent equations. We carefully investigate the effects of the parameters on the final shape of the microelectrodes. Our results are relevant to existing pullers and have important implications for the future design of devices to fabricate microelectrodes.

There are certain similarities between the pulling of the glass microelectrodes and the drawing of optical and polymer fibers, which have been studied extensively in the literature [3, 4, 5, 6, 7]. For example, the governing equations for the extension of the tube or fiber can be obtained by taking the long-wave limit of the Navier–Stokes equation for incompressible fluids. However, most of the fiber drawing literature focuses on the steady state solution and its stability (drawing resonance) under isothermal conditions; cf. [6, 7, 3] and references therein. Nonisothermal cases also have been considered [11, 10, 9], but the focus is on the effect of the temperature variation on the drawing resonance. On the other hand, in the case of making glass microelectrodes, the problem is inherently transient. Another distinctive feature in the electrode pulling case is that the puller normally imposes a constant or variable force, instead of a fixed drawing speed.

Finally, the pulling of microelectrodes also has similar characteristics to extensional flow and break-off of viscous drops, which has been studied extensively; cf. [19] and references therein. However, these studies generally assume that the viscosity of the fluid remains constant, whereas in electrode production temperature-induced viscosity variations are critical.

The rest of the paper is organized as follows. In section 2, we state the basic assumptions and give the model equations. Details of the control-volume approach used in this derivation are similar to those used in [12] and [6] and therefore will be omitted. However, some issues, which have not previously been considered, such as the effects of surface tension on the inner and outer radii during stretching, will be carefully addressed on the basis of dimensional analysis. A general methodology for solving the model equations based on the method of characteristics is given.

In section 3, we obtain analytical solutions for a horizontal puller with fixed pulling force and uniform heating. For more general cases, approximate solutions are obtained using a simple numerical method. The role of parameter values is thoroughly investigated, and a particularly appealing and simple approximate theory is developed

to predict the radius of the tip at breaking. The consequences for puller design and other applications are discussed in section 4.

2. Model for glass microelectrode formation. The basic equations used in this paper to describe the stretching of the glass tube are similar to those derived in [12] for heated tubes and in [6] for isothermal tubes. In this section, we address the assumptions made in [12] and show that the flow equations reduce to those given in [12] when surface tension is negligible and can be further simplified using dimensional analysis. We also will show that the simplified model leads to a Lagrangian formulation, which can be used to compute the solution much more efficiently than the method used in [12].

2.1. Model formulation. We let ρ be the density of the glass and assume that variations in the density with temperature are negligible. We assume the tube is axisymmetric with length ℓ and inner and outer radii r and R, respectively. In the one-dimensional approximation, the velocity of the glass along the axis of the tube, which we denote by u, is independent of the radial position. When the pressure inside and outside the tube are equal, the momentum, mass, and energy conservation laws lead to the following equations:

$$\rho(R^2-r^2)\left(\frac{\partial u}{\partial t}+u\frac{\partial u}{\partial x}-g\right)=\frac{\partial}{\partial x}\left(3\mu(R^2-r^2)\frac{\partial u}{\partial x}+\gamma(R+r)\right), \tag{2.1}$$

$$\frac{\partial R^2}{\partial t}+u\frac{\partial R^2}{\partial x}+R^2\frac{\partial u}{\partial x}=-\frac{\gamma Rr}{\mu(R-r)}, \tag{2.2}$$

$$\frac{\partial r^2}{\partial t}+u\frac{\partial r^2}{\partial x}+r^2\frac{\partial u}{\partial x}=-\frac{\gamma Rr}{\mu(R-r)}, \tag{2.3}$$

$$\rho c_p\left(\frac{\partial \theta}{\partial t}+u\frac{\partial \theta}{\partial x}\right)=E_R, \tag{2.4}$$

where g is the gravitational constant, γ is the surface tension coefficient, t is the time, x is the coordinate measured along the axis of the cylinder, μ is the viscosity of the glass, θ is the temperature, c_p and k are the specific heat and thermal conductivity of the glass, respectively, and E_R represents the transport of thermal energy to the glass tube by radiation. This thermal radiation term is given by

$$E_R=2k_B\sqrt{\frac{\pi}{s(1-\beta^2)}}\left[E_h\frac{\varepsilon_h\alpha}{1-(1-\alpha)(1-\varepsilon_h)}\left(\theta_h^4-\theta^4\right)+E_b\frac{\varepsilon_b\alpha}{1-(1-\alpha)(1-\varepsilon_b)}\left(\theta_b^4-\theta^4\right)\right], \tag{2.5}$$

where $s=\pi(R^2-r^2)$ is the cross-sectional area, $\beta=r/R$ is the ratio of the radii, k_B is the Boltzmann constant, α is the absorptivity of the glass to radiative thermal energy, ε_h and ε_b are the emissivities of the heater and background, respectively, and $\theta_h(x,t)$ and $\theta_b(x,t)$ are the temperatures of the heater and the background, respectively. The quantities E_h and E_b are geometric factors between the heater and the glass tube and between the background and the glass tube, respectively. These geometric factors can be derived by integrating over the surface of the heater (and surrounding body) visible to the element of the glass tube. The details can be found in [12]. The heating is usually applied to a highly localized region of the tube of length $\ell_h \gg R_0$.

These equations are valid if the glass tube is long and thin with a small radius to length aspect ratio, as shown in Table 2.1. In addition, they also require that

the viscosity variation in the radial direction be small compared to that in the axial direction, which is justified since the viscosity is temperature-dependent and the radial variation of temperature is small, compared to that in the axial direction, as shown in Appendix A. The derivation of (2.1)–(2.3) can be found in [6].

The above equations are subject to the following initial and boundary conditions. Initially, we assume that the glass tube has a uniform temperature θ_0, length ℓ_0, and inner and outer radii r_0 and R_0. The tube is being pulled at one end with force $F(t)$, i.e.,

$$3\mu\pi(R^2 - r^2)\frac{\partial u}{\partial x} + \gamma\pi(R + r) = F(t) \tag{2.6}$$

at $x = \ell(t)$, which is a moving boundary with speed

$$\frac{d\ell}{dt} = v, \tag{2.7}$$

where $v = u(\ell, t)$ is the velocity of the glass at $x = \ell$. For symmetric pulling, we apply the condition of symmetry at $x = 0$. For asymmetric pulling with a fixed end, we simply have

$$u = 0 \tag{2.8}$$

at $x = 0$.

For pulling of glass electrodes, we also apply a terminal condition. If the pulling process is successful, the glass tube breaks in the location where the stress exceeds the "breaking stress." The breaking stress is a material-dependent parameter that also depends on the temperature. For example, for the glass used in this study, the breaking stress, $\mathcal{S}_b$, is given by the empirical formula [17]

$$\mathcal{S}_b = \frac{B}{\sqrt{\theta}}, \tag{2.9}$$

where B is an empirically determined constant.[1] The glass tube breaks when the stress in the tube is greater than $\mathcal{S}_b$. We note that this empirical law indicates that it becomes easier to break this type of glass as the temperature increases.

The difference between horizontal and vertical pullers appears only in the boundary conditions. For vertical pullers, one end of the tube is attached to a fixed location while a weight is attached to the other end. In this case, as the tube stretches, the

[1]The concept of breaking stress used in this paper is the same as the strength of glass, explored by Coenen [1]. From observations of the processes in a glass melt during the formation of cavities and of new surfaces, the formula

$$\sigma \approx 27 \times 10^6 \sqrt{\gamma^3/\theta}$$

was given in [17, p. 272]. Here σ is the applied stress (in N/m^2), γ is the surface tension coefficient (in N/m), and θ is the temperature measured in K. The weakening of the glass melt strength is partially caused by the decrease of elastic modulus when the temperature increases. The dominant factor, however, is due to the surface damage that occurs upon heating, which leads to spontaneous fracture. This mechanism is different from the pinch-off of viscous jets, where surface tension is the dominant factor and normally the inner radius collapses. On the other hand, the functional glass microelectrodes produced by the pullers have open annuli at the tips formed by breaking.

By neglecting the temperature-dependence of the surface tension coefficient [17] and using $\gamma = 0.33$ N/m for a soda-lime glass melt at 800° C, we arrive at (2.9), with B given in Table 2.1.

weight accelerates, and so the force experienced by the end of the tube is decreased. We denote the weight by F_0, gravity by g, the distance along the tube from the fixed end by x, and the location of the end attached to the weight by $x = \ell(t)$. We obtain an expression for the force applied to the free end of the tube, $F(t)$, given by

$$F(t) = F_0 - \frac{F_0}{g}\frac{\mathrm{d}^2\ell}{\mathrm{d}t^2}. \tag{2.10}$$

For horizontal pullers, the situation is simpler, and the force applied to the ends of the tube is simply $F(t)$, a specified function of time.

Equations (2.2) and (2.3) can be combined to give an equation for the cross-sectional area, s, which is essentially the equation of mass conservation,

$$\frac{\partial s}{\partial t} + u\frac{\partial s}{\partial x} + s\frac{\partial u}{\partial x} = 0. \tag{2.11}$$

The equations (2.2) and (2.3) also imply that the ratio of the radii, $\beta = r/R$, satisfies

$$\frac{\partial \beta}{\partial t} + u\frac{\partial \beta}{\partial x} = -\frac{\gamma(1+\beta)}{2\mu R}. \tag{2.12}$$

In the rest of the paper, we will use (2.11) and (2.12) instead of (2.2) and (2.3).

In a certain range of glass temperatures, the viscosity varies rapidly, and this plays a fundamental role in controlling the dynamics. Empirical data for soda-lime [2] shows that for temperatures below 900 K, which generally will be the case for electrode formation, the viscosity has an exponential dependence on temperature given by

$$\mu(\theta) = \mu_0 \exp\left[-\frac{(\theta - \theta_0)}{\theta_a}\right], \tag{2.13}$$

where μ_0 is the viscosity at the ambient temperature, θ_0, and θ_a is the "activation temperature change" required to change the viscosity by a factor of e^{-1}.

The parameters for the glass tube and heater are given in Tables 2.1 and 2.2, respectively. The other parameter that is relevant to the puller is the maximum length that the glass can be extended. This is generally constrained by the physical size of the device. If the device does not allow the tube to be extended sufficiently, then the tube may not break, and so no electrode will be formed. In later sections, we will carefully examine how the required amount of extension is related to the other parameters.

In the following sections, we will consider the most complicated case of the vertical puller, where the force on the glass tube is due to a weight that is accelerating under the influence of gravity. The other cases of specified time-dependent forces are simpler, and we will explain how to treat these cases in section 2.5.

TABLE 2.1
List of the physical parameters relating to the glass tube.

ρ g cm^{-3}	c_p Erg K^{-1} g^{-1}	k Erg cm^{-1} s^{-1} K^{-1}	k_B Erg cm^{-2} s^{-1} K^{-4}	ε_h	ε_b	α
2.23	7.538×10^6	1.130×10^5	5.67×10^{-5}	1	1	0.4

ℓ_0 cm	R_0 cm	r_0 cm	μ_0 g cm^{-1} s^{-1}	θ_a K	B dyn cm^{-3} K$^{1/2}$	γ g s^{-2}
7.56	8.66×10^{-2}	4.33×10^{-2}	10^9	50	5×10^{10}	300

TABLE 2.2
List of the geometrical parameters relating to the puller.

ℓ_h cm	F_0 g cm s^{-2}	$\theta_0 = \theta_b$ K	θ_h K
0.3	2×10^5	300	1000

2.2. Dimensional analysis. For the vertical puller, we nondimensionalize the variables using the following scales:

$$u = \frac{\ell_0 F_0}{3\mu_0 s_0} u', \quad s = s_0 s', \quad x = \ell_0 x', \quad t = \frac{3\mu_0 s_0}{F_0} t', \quad F = F_0 F',$$
$$R = R_0 R', \quad \ell = \ell_0 \ell', \quad \theta = \theta_0 + \theta_a \theta', \quad \text{and} \quad \mu(\theta) = \mu_0 \mu'(\theta'), \tag{2.14}$$

where the dimensionless variables are labeled with primes. Here ℓ_0, s_0, R_0, and r_0 are the initial length, cross-sectional area, and the outer and inner radii of the glass tube. Note that we have used

$$u_0 = \frac{\ell_0 F_0}{3\mu_0 s_0}$$

as the velocity scale, by balancing the pulling weight F_0 with the viscous force in the glass tube using the elongation viscosity. After substitution and dropping primes, the momentum equation (2.1), mass conservation equation (2.11), equation for the radii ratio (2.12), and heat equation (2.4) become

$$Re\left(\frac{\partial u}{\partial t} + u\frac{\partial u}{\partial x} - \frac{1}{F_r}\right) = \frac{1}{s}\frac{\partial}{\partial x}\left(\mu s \frac{\partial u}{\partial x} + \lambda R(1+\beta)\right), \tag{2.15}$$

$$\frac{\partial s}{\partial t} + u\frac{\partial s}{\partial x} + s\frac{\partial u}{\partial x} = 0, \tag{2.16}$$

$$\frac{\partial \beta}{\partial t} + u\frac{\partial \beta}{\partial x} = -\frac{3}{2}(1-\beta_0^2)\lambda\frac{(1+\beta)}{\mu R}, \tag{2.17}$$

$$\theta_t + u\theta_x = \mathcal{H}\frac{H(x,\theta)}{s^{1/2}}\sqrt{\frac{1-\beta_0^2}{1-\beta^2}}. \tag{2.18}$$

(The derivation of (2.18) is given in Appendix A.) The dimensionless boundary conditions for the vertical puller are

$$u = 0 \ \text{ at } \ x = 0 \tag{2.19}$$

and

$$\mu s\frac{\partial u}{\partial x} + \lambda R(1+\beta) = 1 - F_r\frac{d^2\ell}{dt^2}, \qquad u = \frac{d\ell}{dt} \ \text{ at } \ x = \ell. \tag{2.20}$$

The initial conditions are

$$u = 0, \ \ s = 1, \ \ \theta = 0, \ \ \ell = 1 \ \text{ at } \ t = 0. \tag{2.21}$$

The terminal condition is the nondimensional breaking criterion

$$\max_{0\le x\le \ell}\left\{\mu s\frac{\partial u}{\partial x} + \lambda R(1+\beta) - \frac{C_b s}{\sqrt{\theta + \frac{\theta_0}{\theta_a}}}\right\} = 0, \tag{2.22}$$

where

$$C_b = \frac{Bs_0}{F_0\sqrt{\theta_a}}.$$

The dimensionless parameters

$$Re = \frac{\rho F_0 \ell_0^2}{9\mu_0^2 s_0}, \quad F_r = \frac{u_0^2}{g\ell_0}, \quad \lambda = \frac{\pi\gamma R_0}{F_0}$$

are the ratio of inertia to viscous forces, the inertia to the gravity forces, and surface tension forces to the external pulling force, respectively. $\beta_0 = r_0/R_0$ is the initial value of β,

$$\mathcal{H} = \frac{6\mu_0\sqrt{s_0}k_B\epsilon_h\alpha\theta_h^4\sqrt{\pi}}{\rho c_p\theta_a F_0\sqrt{(1-\beta_0^2)}[1-(1-\alpha)(1-\epsilon_h)]}$$

is the dimensionless heater strength, and

(2.23)
$$H(x,\theta) = E_h(x)\left(1-\left(\frac{\theta_0+\theta\theta_a}{\theta_h}\right)^4\right) + \frac{\epsilon_b[1-(1-\alpha)(1-\epsilon_h)]E_b(x)(\theta_b^4-(\theta_0+\theta_a\theta)^4)}{\epsilon_h[1-(1-\alpha)(1-\epsilon_b)]\theta_h^4}$$

is the dimensionless radiation distribution. In the case when heater temperature is much higher than that of the glass and the background, then $H(x,\theta)$ can be approximated by a given function of x. The dimensionless heater strength, $\mathcal{H}$, can be thought of as the heat absorbed by a thread being pulled with constant force F_0 as it passes through the heater, divided by the heat required to significantly change the viscosity. Small values of $\mathcal{H}$ imply that the viscosity remains almost constant, and so the solution will be similar to the isothermal case. Large values of $\mathcal{H}$ imply that significant viscosity gradients will occur in the thread. The dimensionless radiation distribution is the normalized radiative heat flux.

We now can further simplify the governing equations based on the parameter estimates at two of the most relevant stages: the beginning of the pulling and when the glass tube breaks. Initially, the tube is cold and the viscosity is large, whereas near breaking, the tube will have absorbed a significant amount of heat, and the viscosity can be reduced by several orders of magnitude. As a consequence, dimensionless variables describing the flow can vary dramatically. Therefore, we need to consider the relative sizes of inertia, gravity, surface tension, and viscous and pulling forces at both stages.

Using the typical parameters in Tables 2.1 and 2.2, we see that dimensionless parameters

$$\lambda \approx 4\times 10^{-4}, \quad Re \approx 1.6\times 10^{-10}, \quad \text{and} \quad Re/F_r \approx 10^{-3}$$

are small, and therefore initially surface tension and inertial and gravitational forces can be ignored. Typically, $\mathcal{H} = O(200)$; therefore initially the heating of the tube dominates the advective term, and the tube temperature increases with very little motion. However, when the tube is heated, the viscosity decreases dramatically, the tube stretches quickly, and the tube diameter decreases rapidly. These large changes mean that the above dimensionless parameters may not adequately characterize the sizes of

the surface tension, inertial and gravitational forces when the tube is close to breaking. We therefore must also compare the inertial, surface tension, and gravitational forces with the size of the imposed force near breaking.

Assuming that the stress in the tube can be approximated by the pulling force divided by the cross-sectional area, the dimensionless breaking criterion for the vertical puller is given by

$$\frac{1}{s}\left(1 - F_r \frac{d^2\ell}{dt^2}\right) = \frac{C_b}{\sqrt{\theta + \frac{\theta_0}{\theta_a}}}. \tag{2.24}$$

We first must obtain order of magnitude estimates for the diameter at which the tube breaks, the highest temperature that the tube reaches, and the viscosity of the tube near breaking. The tube starts to stretch significantly when the advection and radiative heating terms are of the same order of magnitude. This means that the viscosity must drop by a factor of order $\mathcal{H} = 200$. Hence, the viscosity near breaking μ_b will be of order $1/200$, and the dimensionless temperature must rise by approximately 6 (which corresponds to a dimensional temperature change of approximately 300 K). Knowing the temperature, θ, and using the breaking stress formula (2.24), we can obtain an order of magnitude estimate for the dimensionless cross-sectional area at which breaking occurs, s_b, yielding $s_b = 10^{-2}$ (which corresponds to a dimensional cross-sectional area of order 10^{-4} cm^2).

We are now in a position to estimate the dimensionless ratios near the breaking time. Using (2.15) and (2.20), we see that the characteristic sizes of the surface tension and inertial and gravitational terms compared to the imposed force are given by

$$s_b^{1/2}\lambda = O(10^{-5}), \quad \frac{1}{\mu_b^2 s_b} Re = O(10^{-3}), \quad \text{and} \quad s_b \frac{Re}{F_r} = O(10^{-5}),$$

respectively. Therefore, we can conclude that surface tension, inertia, and gravity can be neglected during the entire pulling process. The acceleration term, $F_r\ d^2\ell/dt^2$, is negligible initially because it is $O(10^{-7})$, but near the breaking time, this term may be O(1), and so we must retain this term. Similarly, the ratio of the initial stress to the breaking stress, C_b, is $O(10^2)$, indicating that the tube is initially far from breaking, but eventually the tube will become sufficiently thin that the stress will approach the breaking stress.

We note that the above discussion considers only the case of successful pulling of microelectrodes; i.e., the breaking criterion is met during the extension of the glass tube. In practice, this is not always the case, and it is possible that the glass continues to extend without breaking. When this occurs, the glass may become very heavily extended, and the acceleration term $F_r\ d^2\ell/dt^2$ may approach unity. In this case, the inertia, surface tension, and the gravity may become important. Even though this is an interesting problem, it is not really relevant to successful production of glass microelectrodes and will not be pursued in this paper.

2.3. Eulerian formulation. If the surface tension terms are neglected in (2.17), we immediately see that β is conserved following material elements. We will make the natural assumption that the initial radii, r_0 and R_0, of the tube are uniform, and therefore, β will be a constant throughout the pulling process.

As a result of neglecting inertia, surface tension, and gravity, (2.15) becomes

$$(\mu(\theta) s u_x)_x = 0. \tag{2.25}$$

Since β is constant, the heat equation (2.18) reduces to

$$\theta_t + u\theta_x = \mathcal{H}\frac{H(x,\theta)}{s^{1/2}}. \tag{2.26}$$

Equations (2.25) and (2.26), combined with the mass equation

$$s_t + us_x + su_x = 0, \tag{2.27}$$

form a closed system. The glass tube does not break as long as the inequality

$$\frac{1}{s}\left(1 - F_r\frac{d^2\ell}{dt^2}\right) < \frac{C_b}{\sqrt{\theta + \frac{\theta_0}{\theta_a}}} \tag{2.28}$$

is valid for all x. If this criterion is violated, then the tube will break and the stretching process is terminated.

For vertical pullers, a mass is attached to one end of the glass tube. Thus, the pulling force $F(t)$ is determined by Newton's second law, in nondimensional form as

$$F(t) = 1 - F_r\frac{d^2\ell}{dt^2}. \tag{2.29}$$

The boundary condition is

$$\mu(\theta)su_x|_{x=\ell} = F(t). \tag{2.30}$$

For horizontal pullers, the pulling force $F(t)$ is externally prescribed. For a constant force puller, this is equivalent to setting $F_r = 0$ in (2.29).

The momentum equation (2.25) can be integrated as

$$\mu(\theta)su_x = 1 - F_r\frac{\mathrm{d}^2\ell}{\mathrm{d}t^2}. \tag{2.31}$$

Dividing this equation by $s\mu(\theta)$ and integrating from $x = 0$ to ℓ gives an expression for the velocity of the free end, denoted by v,

$$v(t) = u(\ell,t) = \frac{d\ell}{dt} = \left(1 - F_r\frac{\mathrm{d}v}{\mathrm{d}t}\right)\int_0^\ell \frac{\mathrm{d}\eta}{s(\eta,t)\mu(\theta(\eta,t))}. \tag{2.32}$$

This can be rewritten as a differential equation for v,

$$F_r\frac{\mathrm{d}v}{\mathrm{d}t} = 1 - v\left(\int_0^\ell \frac{\mathrm{d}\eta}{s(\eta,t)\mu(\theta(\eta,t))}\right)^{-1}. \tag{2.33}$$

Using (2.31) and (2.33), the mass equation (2.27) can be reduced to

$$s_t + us_x = -\frac{v}{\mu}\left(\int_0^\ell \frac{\mathrm{d}\eta}{s(\eta,t)\mu(\theta(\eta,t))}\right)^{-1}. \tag{2.34}$$

Finally, the temperature equation is unchanged as

$$\theta_t + u\theta_x = \mathcal{H}\frac{H(x,\theta)}{s^{1/2}}. \tag{2.35}$$

Equations (2.33)–(2.35) can be solved subject to the initial conditions

$$s = 1,\ \theta = 0,\ \ell = 1,\ u = 0,\ v = 0 \quad \text{at} \quad t = 0. \tag{2.36}$$

2.4. Lagrangian formulation. As shown in [20, 13, 19], the system of equations becomes significantly simpler if expressed in Lagrangian coordinates (ξ, τ). The relationship between the Lagrangian and Eulerian coordinates is given by $x = X(\xi, \tau)$ and $t = \tau$, and

$$x_\tau = \frac{\partial X(\xi, \tau)}{\partial \tau} = u. \tag{2.37}$$

When there is no ambiguity, we will use x as both Eulerian coordinate and the Lagrangian variable X, which is the spatial coordinate of a material point which was at the location $x = \xi$ at the initial time $\tau = 0$.

For a function $f(x, t)$ defined using Eulerian coordinates, its Lagrangian derivatives are

$$f_\tau = f_t + f_x x_\tau = f_t + u f_x, \qquad f_\xi = f_x x_\xi. \tag{2.38}$$

It follows immediately that

$$u_x = \frac{u_\xi}{x_\xi} = \frac{x_{\tau\xi}}{x_\xi}. \tag{2.39}$$

Using (2.38) and (2.39), the conservation-of-mass equation (2.16) can be rewritten as

$$s_\tau + s\frac{x_{\tau\xi}}{x_\xi} = 0 \rightarrow (s x_\xi)_\tau = 0.$$

Integrating and applying the initial conditions, $s(\xi, 0) = 1$ and $x(\xi, 0) = \xi$, gives

$$x_\xi = \frac{1}{s}. \tag{2.40}$$

Writing $\mu(\theta) = e^{-\theta}$ and using Lagrangian coordinates, (2.33)–(2.35) become

$$F_r\, v_\tau(\tau) = 1 - v(\tau)\left(\int_0^1 s(\eta, \tau)^{-2} e^{\theta(\eta,\tau)} \mathrm{d}\eta\right)^{-1}, \tag{2.41}$$

$$s_\tau(\xi, \tau) = -v(\tau) e^{\theta(\xi,\tau)}\left(\int_0^1 s(\eta, \tau)^{-2} e^{\theta(\eta,\tau)} \mathrm{d}\eta\right)^{-1}, \tag{2.42}$$

and

$$\theta_\tau(\xi, \tau) = \mathcal{H}\frac{H(x(\xi, \tau), \theta(\xi, \tau))}{s(\xi, \tau)^{1/2}}. \tag{2.43}$$

2.5. Horizontal puller with a specified time-dependent force. For the horizontal puller, we need specify only the time-dependent force, $F(t)$, applied to the ends of the tube. We use the same nondimensionalizations specified in (2.14), except that now F_0 would be the maximal value of $F(t)$ over the entire time period of application.

The dimensionless (2.22) then is replaced by the simpler expression

$$\frac{F(t)}{s} = \frac{C_b}{\sqrt{\theta + \frac{\theta_0}{\theta_a}}},$$

where on the left-hand side $F(t)$ is a dimensionless specified function of time. We note that for a horizontal puller with a constant force, the dimensionless force is given by $F(t) = 1$.

In the constant force case, setting $F_r = 0$ in (2.41) leads to an equation for the velocity at the free end, which is given by the algebraic equation

$$v(t) = \int_0^\ell \frac{\mathrm{d}\eta}{s(\eta, t)\mu(\theta(\eta, t))}. \tag{2.44}$$

In Lagrangian coordinates with $\mu(\theta) = e^{-\theta}$, the velocity at the free end is given by

$$v(\tau) = \int_0^1 s(\eta, \tau)^{-2} e^{\theta(\eta,\tau)} \mathrm{d}\eta. \tag{2.45}$$

Then (2.42) and (2.43) reduce to

$$s_\tau = -\frac{1}{\mu(\theta)} = -e^\theta \tag{2.46}$$

and

$$\theta_\tau = \frac{\mathcal{H}}{\sqrt{s}} H(x(\xi, \tau), \theta). \tag{2.47}$$

2.6. Numerical method. For a general heating profile or for time-dependent pulling forces, no explicit solutions can be obtained, and we must resort to numerical methods. For an arbitrary heating profile, $H(x, \theta)$, the equations (2.41)–(2.43) can be used as the basis for a simple numerical method. The Lagrangian description of the system allows us to implement a very simple numerical method that completely avoids the problem of numerical diffusion, which arises in finite difference methods.

In order to solve this problem, we discretize the domain in both ξ and τ. At any given time τ, we use the trapezoidal rule to compute the integral $\int_0^1 s^{-2} e^\theta \mathrm{d}\xi$. Having done this, we then integrate the system of equations given in (2.41)–(2.43) using an ODE solver, e.g., a simple Euler method. Since the heater profile is given in Eulerian coordinates, we need to know the location of the material point, which can be computed using a numerical quadrature of (2.40). We note that this method can cope easily with generalized heating profiles, asymmetrical pulling, variable pulling forces, and the inclusion of heat exchange terms, θ_a^4/θ_h^4.

3. Results. In this section, we consider a number of possible configurations for the puller and heating profiles. We begin with a symmetric puller with a heater that supplies spatially constant heating. In this case, we can derive an analytical solution of the equations, and this allows us to understand many of the important features leading to the shape formation of the electrode. We then go on to consider a symmetric puller with nonuniform heating, an asymmetric puller with nonuniform heating, and finally a vertical puller.

3.1. Symmetrical pulling with constant force and constant heating. In this section, we consider the case when the pulling force is a constant, that is, a horizontal puller. We assume that the pulling and heating are symmetric about $x = 0$, and so the velocity at $x = 0$ is zero by symmetry. Therefore, the point that is initially at the centerline, $\xi = 0$, will always correspond to the point $x = 0$. Since there is no direct coupling between the breaking criterion and the shape evolution, we

will derive the solution by initially computing the shape profile and then determining the time at which the breaking criterion is first satisfied.

In order to obtain an explicit solution, we make a physically relevant assumption about the heater profile that provides a number of important insights into the problem. We will assume that the tube is initially located in the region $-1/2 \le x \le 1/2$ and that the heater is localized to the region $-\ell_h/2 \le x \le \ell_h/2$, where $0 < \ell_h < 1$ is the length of the heater. We also assume that the geometric factor, $E_h(x)$, is a constant in the heater region and zero outside of the heater region. This is appropriate if the radius of the heater element is not much larger than the outer radius of the tube. Since the glass achieves a peak temperature that typically is significantly less than the heater temperature, we will neglect the terms that are $O(\theta_a^4/\theta_h^4)$. Hence, we approximate the heating in the heater region by a constant. After the tube absorbs a significant amount of heat, it is stretched rapidly before it breaks, and so there is very little time for cooling to occur outside of the heater region. This means that we can safely neglect the cooling terms.

Therefore, the heater profile is assumed to be piecewise constant, that is,

$$H(x) = \begin{cases} 1 & 0 \le x \le \ell_h/2, \\ 0 & x > \ell_h/2. \end{cases} \tag{3.1}$$

We now discuss the solution of (2.40), (2.46), and (2.47) when $H(x)$ is given by (3.1). For any time τ, there are three parts of the solution that need to be considered separately.

Region (i). We first consider material points that are initially in the heater region and remain in the heater region at time τ. We define $\tau_h(\xi)$ to be the solution of $x(\xi, \tau_h(\xi)) = \ell_h/2$, which represents the time that a material element that starts at $x = \xi$ exits the heater region (see Figure 3.1). When $\tau < \tau_h(\xi)$, the material element

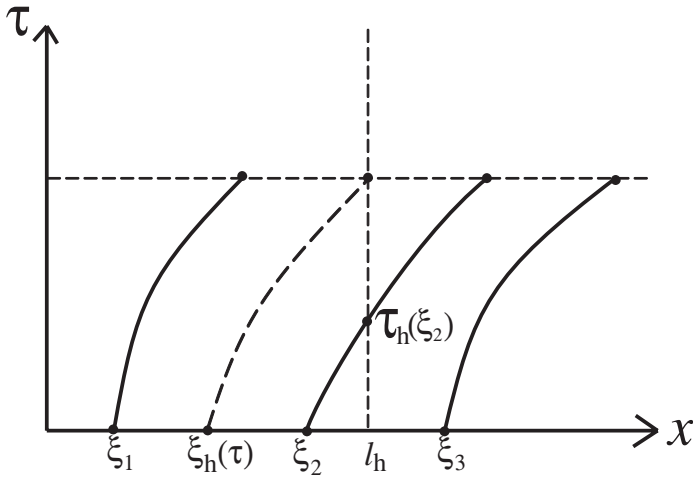

FIG. 3.1. *Symmetrical pulling with constant force and constant heating. Lagrangian trajectories.*

is subject to constant heating; thus, we need to solve the following equations:

$$s_\tau = -e^\theta, \quad \theta_\tau = \frac{\mathcal{H}}{\sqrt{s}}, \quad \text{and} \quad s x_\xi = 1, \tag{3.2}$$

subject to $s = 1$, $\theta = 0$, and $x = \xi$ at $\tau = 0$.

From (3.2), we obtain

$$\frac{\partial s}{\partial \theta} = -\frac{\sqrt{s} e^\theta}{\mathcal{H}}. \tag{3.3}$$

Integrating and applying the initial conditions yields

$$\sqrt{s} = \frac{1 + 2\mathcal{H} - e^\theta}{2\mathcal{H}}. \tag{3.4}$$

Substituting (3.4) into (3.2), we obtain

$$s_\tau = 2\mathcal{H}\sqrt{s} - (1 + 2\mathcal{H}) \quad \text{and} \quad \theta_\tau = \frac{2\mathcal{H}^2}{2\mathcal{H} + 1 - e^\theta}. \tag{3.5}$$

These two equations can be integrated again, and after applying the boundary conditions, we obtain

$$(2\mathcal{H} + 1)\theta - e^\theta + 1 = 2\mathcal{H}^2 \tau, \tag{3.6}$$

$$\sqrt{s} - 1 + \frac{2\mathcal{H} + 1}{2\mathcal{H}} \ln\left(2\mathcal{H} + 1 - 2\mathcal{H}\sqrt{s}\right) = \mathcal{H}\tau. \tag{3.7}$$

These equations can be solved explicitly in terms of the Lambert-W function that satisfies $W(x)e^{W(x)} = x$ to give

$$\theta = \frac{2\mathcal{H}^2\tau - 1}{2\mathcal{H} + 1} - W\left(-\frac{\exp\left(\frac{2\mathcal{H}^2\tau - 1}{2\mathcal{H}+1}\right)}{2\mathcal{H} + 1}\right) \tag{3.8}$$

and

$$s = \left(\frac{2\mathcal{H} + 1}{2\mathcal{H}}\right)^2 \left[1 + W\left(-\frac{\exp\left(\frac{2\mathcal{H}^2\tau - 1}{2\mathcal{H}+1}\right)}{2\mathcal{H} + 1}\right)\right]^2. \tag{3.9}$$

The Lambert function is defined only for values $x \geq -e^{-1}$. At the point $x = -e^{-1}$, its value is $W = -1$, and its gradient becomes singular. If the glass tube is allowed to extend, this singularity occurs at the finite time

$$\tau_{pinch} = \frac{(2\mathcal{H} + 1)\ln(2\mathcal{H} + 1) - 2\mathcal{H}}{2\mathcal{H}^2} \tag{3.10}$$

and corresponds to a pinch-off. However, in the case of pulling electrodes, pinch-off does not happen for the following reason. Note that at pinch-off, the cross-sectional area tends to zero, while the extension tends to infinity. In Figure 3.2, we plot the time at which pinch-off occurs as a function of the heating rate $\mathcal{H}$. We see that increasing the heating rate $\mathcal{H}$ causes the viscosity to decrease, and so the tube pinches off more quickly. In fact, this pinch-off will never occur because the stress in the tube will tend

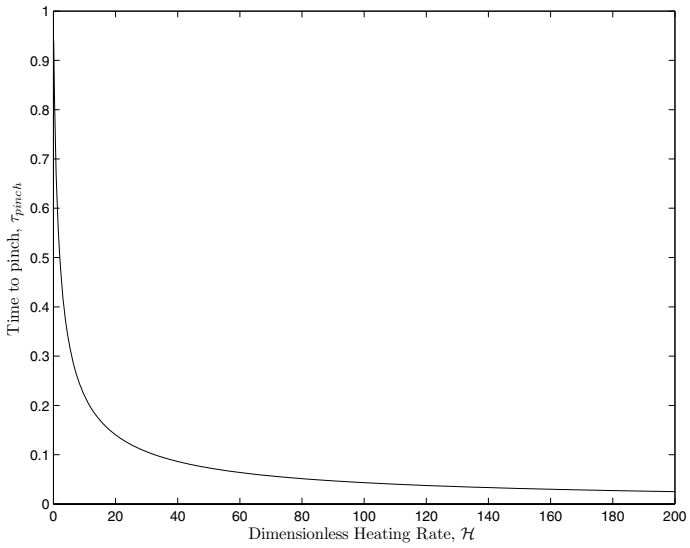

FIG. 3.2. *Dimensionless time to pinch-off as a function of the dimensionless heating rate.*

to infinity, hence exceeding the breaking stress. This means that the tube will always break before a pinch-off can occur. The time for pinch-off represents an upper bound on the duration of the pull. We will return with a more detailed discussion on the breaking of the glass tube after presenting the solutions for regions (ii) and (iii).

We note that in Lagrangian coordinates, the cross-sectional area, s, and the temperature, θ, are functions of τ only. Therefore, at time τ, we can use (3.2) to find the location of a material element that started at $x = \xi$ to obtain

$$x(\xi, \tau) = \int_0^{\xi} \frac{1}{s(\tau)} d\eta = \frac{\xi}{s(\tau)}. \tag{3.11}$$

Hence, a material element that started at $x = \xi$ will exit the heater region at a time $\tau_h(\xi)$, which can be found by solving

$$s(\tau_h(\xi)) = \frac{2\xi}{\ell_h}. \tag{3.12}$$

Substituting the above equation into (3.7), we find that

$$\tau_h(\xi) = \frac{1}{\mathcal{H}} \left[\sqrt{\frac{2\xi}{\ell_h}} - 1 + \frac{1 + 2\mathcal{H}}{2\mathcal{H}} \ln \left(2\mathcal{H} + 1 - 2\mathcal{H} \sqrt{\frac{2\xi}{\ell_h}} \right) \right]. \tag{3.13}$$

Note that points that were initially arbitrarily close to the center will exit the heater region when the time is sufficiently close to the pinching time.

In order to obtain the solution in the next region, we need the temperature of the material element that exits the tube at $\tau = \tau_h(\xi)$. This can be obtained by solving (3.4) and (3.12) to yield

$$\theta(\tau_h(\xi)) = \ln \left(2\mathcal{H} + 1 - 2\mathcal{H} \sqrt{\frac{2\xi}{\ell_h}} \right). \tag{3.14}$$

Region (ii). We now consider material points that are initially inside the heater region but exit the heater region before time τ. In other words, this region contains particles ξ for which $\tau_h(\xi) < \tau$. In this case, we can obtain the solution in a way similar to that used for region (i). Over the time interval $(0, \tau_h(\xi)]$, the solution for these particles is as given in region (i), while for the time interval $(\tau_h(\xi), \tau)$, the solution can be obtained as follows. Since the heating rate is zero, the temperature remains constant at $\theta(\tau_h(\xi))$. Therefore, the equations reduce to

$$s_\tau = -e^{\theta(\tau_h(\xi))} \quad \text{and} \quad s x_\xi = 1, \tag{3.15}$$

subject to $s = 2\xi/\ell_h$ and $x = \ell_h/2$ at $\tau = \tau_h(\xi)$. These can be solved easily to obtain

$$\theta(\xi, \tau) = \ln\left(2\mathcal{H} + 1 - 2\mathcal{H}\sqrt{\frac{2\xi}{\ell_h}}\right), \tag{3.16}$$

$$s(\xi, \tau) = \frac{2\xi}{\ell_h} - \left(2\mathcal{H} + 1 - 2\mathcal{H}\sqrt{\frac{2\xi}{\ell_h}}\right)(\tau - \tau_h(\xi)), \tag{3.17}$$

where $\tau_h(\xi)$ is given in (3.13). At time τ, we can find the location of a material element that started at $x = \xi$ using

$$x(\xi, \tau) = \frac{\ell_h}{2} + \int_{\xi_h(\tau)}^{\xi} \frac{1}{s(\eta, \tau)} d\eta, \tag{3.18}$$

where s is given in (3.17) and $\xi_h(\tau)$ is the original location of the material point that exits the heater at time τ. An explicit expression for $\xi_h(\tau)$ can be obtained by solving (3.13) to yield

$$\xi_h(\tau) = \frac{\ell_h}{2}\left(\frac{2\mathcal{H}+1}{2\mathcal{H}}\right)^2 \left(1 + W\left[-\frac{\exp\left(\frac{2\mathcal{H}^2\tau - 1}{2\mathcal{H}+1}\right)}{2\mathcal{H}+1}\right]\right)^2. \tag{3.19}$$

Region (iii). We finally consider material points that are initially outside the heater region, that is, $\ell_h/2 < \xi \leq 1/2$. These points are never exposed to the heater; therefore, the temperature remains at zero. Thus, the equation for the cross-sectional area (2.42) becomes $s_\tau = -1$, which can be integrated once to yield

$$s = 1 - \tau.$$

Finally, (2.40) can be integrated to yield

$$x(\xi, \tau) = x\left(\frac{\ell_h}{2}, \tau\right) + \frac{\xi - \ell_h/2}{1 - \tau}.$$

Breaking criterion. In order to successfully make a microelectrode, the glass tube must break before the end of the tube reaches the maximum travel distance, ℓ_{max}. We begin by computing the time at which breaking occurs, τ_b. We use the solution obtained above along with the breaking criterion

$$\frac{1}{s_b}\sqrt{\theta_b + \frac{\theta_0}{\theta_a}} = C_b.$$

In the symmetric pulling case, the minimum cross-sectional area and maximum temperature occur at all the material points that have not yet exited the heater region at τ_b (region (i)). Thus, in principle, the tube can break at any of these material points. Since this region has uniform radii and the length of the region is small and of the same length as the heater, the ambiguity has little effect on the final tip radius of the electrode. For simplicity, we assume that the breaking will occur at $x = 0$, even though our model predicts that the glass tube can break anywhere in the heater region since the stress is the same. This is due to the fact that we have assumed that the heater strength is the same and the tube has uniform initial radii. In practice, of course, the middle of the heater is most likely to be the hottest; therefore, the glass will probably break in the middle. Using the solution obtained earlier, (3.4), the cross-sectional area at which breaking occurs, s_b, can be found by solving

$$\left[C_b^2 s_b^2 - \frac{\theta_0}{\theta_a}\right] = \ln\left[2\mathcal{H}(1-\sqrt{s_b})+1\right]. \tag{3.20}$$

If the tube is preheated such that $\theta_0 \gg \theta_a$, then this equation can be solved explicitly. Otherwise, it must be solved numerically, and this does not pose any serious challenges.

Having obtained s_b, we can compute the electrode profile at breaking. We first compute the time at which the tube breaks, τ_b,

$$\tau_b = \frac{1}{\mathcal{H}}\left[\sqrt{s_b} - 1 + \frac{2\mathcal{H}+1}{2\mathcal{H}}\ln\left(2\mathcal{H}+1-2\mathcal{H}\sqrt{s_b}\right)\right]. \tag{3.21}$$

Given τ_b, the initial location of the material element that is exiting the heater as the breaking occurs, $\xi_h(\tau_b)$, is obtained from (3.19). At breaking, the cross-sectional area profiles in the three different regions can be obtained using the formulas given earlier.

(i) In the heater region, $0 < \xi \le \xi_h(\tau_b)$, the cross-sectional area is independent of location and is given by $s = s_b$.

(ii) For points that were initially in the heater region but exited before breaking, $\xi_h(\tau_b) < \xi \le \ell_h/2$, the solution is given parametrically by

$$s(\xi,\tau_b) = \frac{2\xi}{\ell_h} - \left(2\mathcal{H}+1-2\mathcal{H}\sqrt{\frac{2\xi}{\ell_h}}\right)\left[\tau_b - \tau_h(\xi)\right], \tag{3.22}$$

$$x(\xi,\tau_b) = \frac{\ell_h}{2} + \int_{\xi_h(\tau_b)}^{\xi} \frac{1}{s(\eta,\tau_b)}d\eta, \tag{3.23}$$

where $\tau_h(\xi)$ is given in (3.13) and $\xi_h(\tau_b)$ is given in (3.19).

(iii) For material elements that were initially outside the heater region, $\ell_h/2 < \xi \le 1/2$, the cross-sectional area is also independent of location and is given by

$$s(\xi,\tau_b) = 1 - \tau_b.$$

The total extension of the glass tube is given by

$$x(1/2,\tau_b) = x\left(\frac{\ell_h}{2},\tau_b\right) + \frac{1-\ell_h}{2(1-\tau_b)}.$$

With the analytical expressions for the solution, we are in a position to discuss how to control the final electrode shape. First, we must ensure that the apparatus is long enough to allow sufficient extension so that breaking can occur, that is, $\ell_{max} > x(1, \tau_b)$. If breaking occurs, then each resulting electrode is composed of three parts: a region of length $\ell_h/2$ near the tip of the electrode with constant cross-sectional area s_b, a region from $x(\ell_h/2, \tau_b)$ to the end of the electrode with constant cross-sectional area $1 - \tau_b$, and a region of width $x(\ell_h/2, \tau_b) - \ell_h/2$ that connects these two regions. All of these quantities can be easily computed, and this allows one to determine puller settings to control the shape of the resulting tip.

In the following figures, we consider a heater with dimensionless length, $l_h = 0.5$, with a constant heating rate. In Figures 3.3 and 3.4, we plot the outer radius of the glass tube and the temperature as functions of the distance along the axis at various times before breaking and at the time of breaking. Initially, the glass is cool and the viscosity is relatively high, and so the glass tube deforms very little. However, after some time, the glass in the heater region becomes heated, and therefore the viscosity in this region drops. The dots in the figure show the evolution of material points that initially were spaced uniformly along the tube. From this, it is clear that the vast majority of the deformation occurs to material elements that initially were in the heater region.

We also see that as the breaking point is approached, the stretching occurs very quickly. This can be seen even more clearly in Figure 3.5, where we plot the minimum radius, which in this case occurs at the centerline, as a function of time. For the majority of the time, the material thins slowly, but once stretching begins, it occurs extremely rapidly. If we had ignored the breaking criteria, a pinching event would have occurred when the radius became zero. From this, it is clear that the breaking time can be well approximated by the time at which pinching occurs.

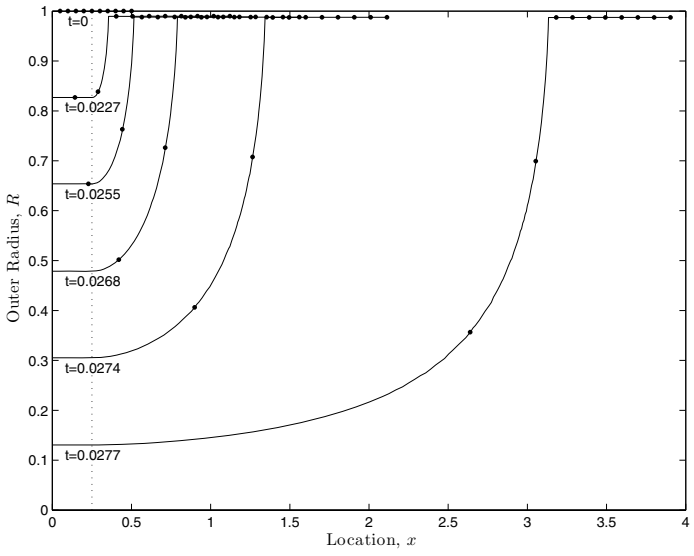

FIG. 3.3. *Outer radius of the glass tube as a function of position. The heater is located between* $x = 0$ *and* $x = 0.25$ *as indicated by the dotted line. The dots in this and subsequent figures show the evolution of material points that initially were spaced uniformly along the tube.*

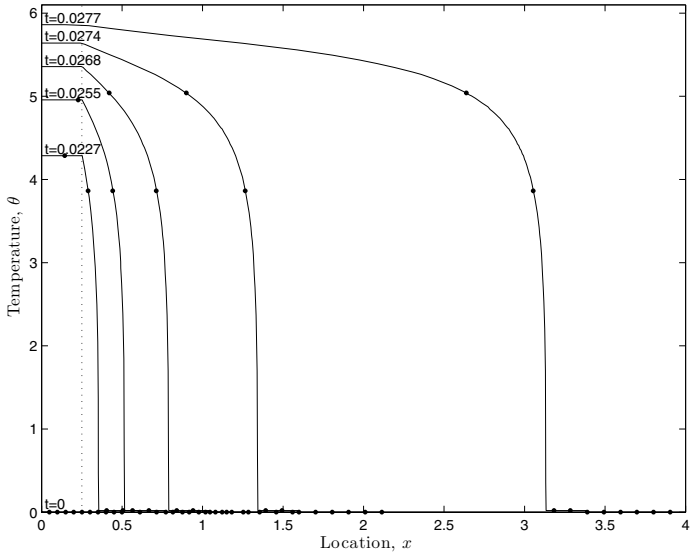

FIG. 3.4. *Temperature of the glass tube as a function of position. The heater is located between* $x = 0$ *and* $x = 0.25$ *as indicated by the dotted line.*

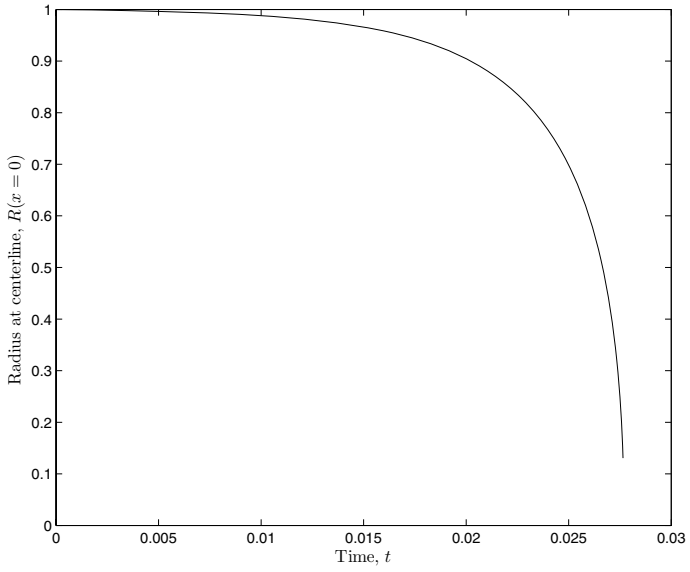

FIG. 3.5. *Minimum radius of the glass tube at the origin as a function of time.*

In Figure 3.6, we plot the dimensionless stress in the glass tube and the dimensionless breaking stress at the centerline as a function of time. As the glass tube thins, the stress increases dramatically, but breaking also is aided by heating, which acts to decrease the breaking stress. Nevertheless, during the time near breaking, the dynamics is dominated by increases in the stress.

3.2. Approximation of tip cross-sectional area. A distinct feature of the glass electrode formation process is the existence of two different regimes if the heating rate $\mathcal{H}$ is large. At early times, the glass is heated, but the viscosity is sufficiently large

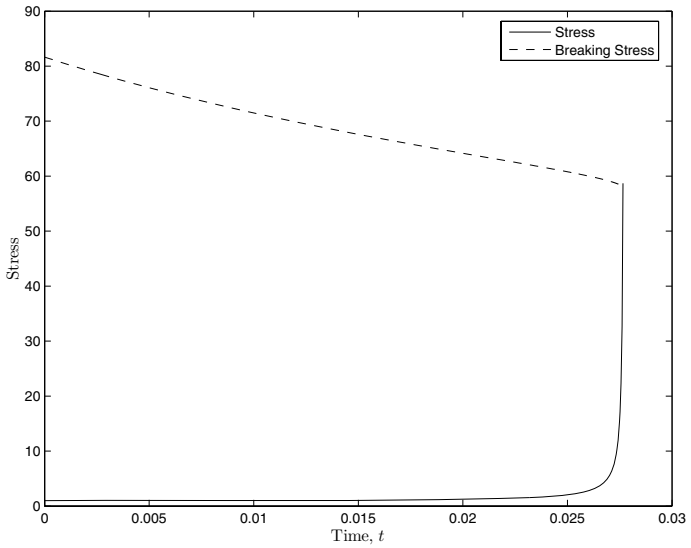

FIG. 3.6. *Dimensionless stress in the glass tube and the dimensionless breaking stress at the centerline as functions of time.*

that little stretching occurs. When the glass has absorbed sufficient thermal energy, the viscosity drops dramatically, and the glass stretches rapidly before breaking. This is largely due to two facts: the relatively large heater strength $\mathcal{H}$ and the exponential dependence of the viscosity on temperature. In the following, we will explain briefly how to use a local asymptotic analysis to obtain approximate solutions for these two regimes.

We start by examining (3.7) for the cross-sectional area s. For a more general case with nonuniform heater strength, we could apply the same local analysis to the set of governing equation (3.2). For simplicity, we will discuss only the case of constant heater strength. When $\mathcal{H} \gg 1$, we can distinguish two cases, i.e., $s \approx 1$ and $s \ll 1$.

3.2.1. Case 1: $s \approx 1$. When $s \approx 1$, or more precisely, $\sqrt{s} = 1 - o(\mathcal{H}^{-1})$, the first two terms in (3.7) essentially cancel, and the remaining two terms are in balance

$$\ln[1 + 2\mathcal{H}(1 - \sqrt{s})] = \mathcal{H}\tau,$$

which yields

$$s \approx 1 - \frac{e^{\mathcal{H}\tau} - 1}{\mathcal{H}}. \tag{3.24}$$

This approximation is valid from $\mathcal{H}\tau = 0$ up to $\mathcal{H}\tau = O(\ln 2\mathcal{H})$. Using (3.6), we find that during this regime the temperature rises from zero to $\theta \approx \ln(2\mathcal{H})$.

3.2.2. Case 2: $s \ll 1$. Near breaking, the glass tube has stretched significantly at the center and the cross-sectional area s tends to zero. Use of (3.7) yields the following approximation:

$$\sqrt{s} - 1 + \ln(1 + 2\mathcal{H}) + \ln\left(1 - \frac{2\mathcal{H}\sqrt{s}}{1 + 2\mathcal{H}}\right) = \mathcal{H}\tau.$$

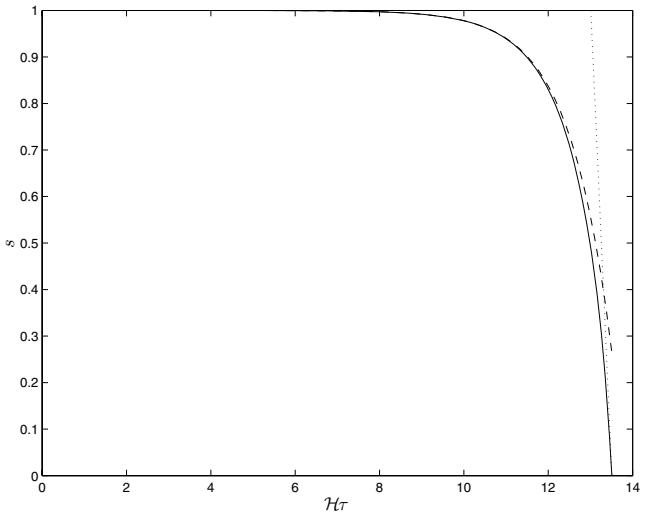

FIG. 3.7. *The cross-sectional area s is plotted as a function of the scaled time $\mathcal{H}\tau$ for a large value of $\mathcal{H} = 10^6$. The solid curve represents the exact solution, while the dashed curve represents the local asymptotic solution for $1 - s \ll 1$,* (3.24)*, and the dotted curve represents the local asymptotic solution for $s \ll 1$,* (3.25)*. The thread heats up with little thinning for a period of time $\tau = O(\mathcal{H}^{-1} \ln(2\mathcal{H}))$ and then thins over a period of time $\tau = O(\mathcal{H}^{-1})$.*

Expanding the logarithmic function in $\sqrt{s}$ yields

$$s \approx 2\ln(1 + 2\mathcal{H}) - 2(\mathcal{H}\tau + 1). \tag{3.25}$$

If the tube were not to break, it would pinch off at time

$$\tau = \frac{\ln(1 + 2\mathcal{H}) - 1}{\mathcal{H}}.$$

Hence, rapid stretching occurs within a relatively short period of time of $O(\mathcal{H}^{-1})$. This is much shorter than the initial phase, which lasted for a time on the order of $O(\mathcal{H}^{-1} \ln(2\mathcal{H}))$. Based on the approximate pinching time, temperature at pinch-off can be approximated by $\theta \approx \ln(2\mathcal{H} + 1)$. Thus the temperature variation during rapid stretching is much smaller than the $\ln(2\mathcal{H})$ variation that occurred in the initial phase.

In Figure 3.7, we have plotted the approximate solutions (3.24) and (3.25) and the exact solution (3.7). The local asymptotic solutions approximate the exact solution well in each regime.

3.2.3. Cross-sectional area at breaking. We now can find approximations that allow us to easily control the shape of the tip. The minimum area of the electrode, s_b, will be significantly smaller than the initial area of the tube; therefore, the breaking time occurs quite close to the pinch-off time. As discussed earlier, at the pinching time, the temperature is given by $\theta \approx \ln(2\mathcal{H} + 1)$. This temperature is also a good approximation for the temperature near the breaking time, because in the time between breaking and pinch-off the change in temperature is small. Hence, the breaking criterion is well approximated by

$$s_b \approx \frac{\sqrt{\ln(2\mathcal{H} + 1) + \theta_0/\theta_a}}{C_b}.$$

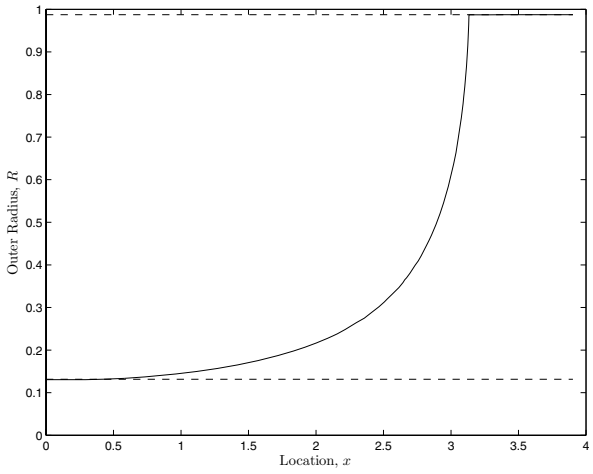

FIG. 3.8. *Microelectrode shape at the breaking time. Also included are the approximations for the tip width and the width of the glass tube far from the tip.*

Also, the area far from the tip, $1 - \tau_b$, can be approximated by $1 - \tau_{pinch}$ as the difference is $O(\mathcal{H}^{-1})$.

In Figure 3.8, we plot the final shape of the electrode along with the approximations to the tip width and the width far from the tip. They can be seen to be in excellent agreement, and this is the case over a wide range of parameters, especially for the tip width. We also have computed the difference between the two solutions, which is less than 2%.

3.3. Symmetric pulling with constant force and nonuniform heating. In this case, we also consider a tube that is initially located in the region $-1/2 \leq x \leq 1/2$ and a puller that is the same as in the above section except that the heating is spatially nonuniform. Rather than use a constant heating profile, we use the profile

$$H(x) = \exp(-4\pi x^2/l_h^2).$$

This has the property that the maximum heater intensity and the integrated heat intensity, $\int H(x)\mathrm{d}x$, are the same as for the piecewise constant heating used in the previous section.

In Figure 3.9, a numerical solution of the final shape of the electrode at the breaking time (solid line) is plotted along with the approximate theory for the tip radius and the radius far from the tip (horizontal dotted lines). In Figures 3.10 and 3.11, we plot the evolution of the outer radius and temperature. We see that the evolution of the glass tube profile is somewhat similar to that for the constant heating case. Of particular interest is the fact that the approximate theory for the uniform heating case still gives an extremely accurate approximation to the final tip radius. This can be understood by again dividing the dynamics into two stages: the first stage in which the glass heats up with little deformation and the second stage in which significant deformation takes place. We consider material elements near the location of the maximum in the heater intensity. In the first stage these points heat up with very little motion of the glass tube. Thus, the temperatures in the uniform and nonuniform calculations are almost identical. Then, since there is very little heating in the second stage, the breaking criteria will be achieved at approximately

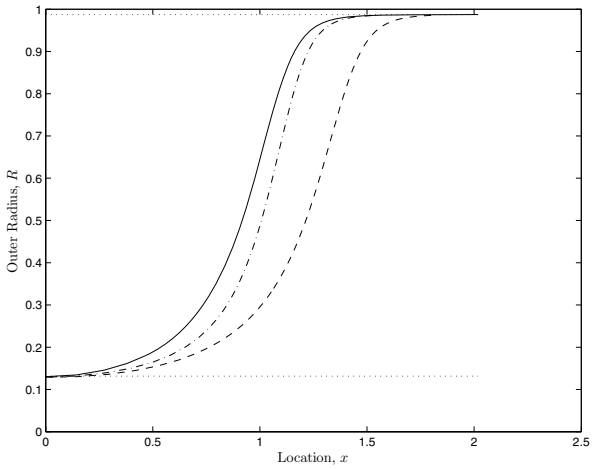

FIG. 3.9. *Final shapes at the breaking times of the microelectrodes for nonuniform heating. Profiles are given for the symmetrical pulling case (solid curve) and for the asymmetrical pulling case (dash-dot curve for the microelectrode formed from the part of the glass tube that remains attached to the fixed wall, dashed curve for the microelectrode formed by the part of the tube which is being pulled). Also, the tip radius and the radius far from the tip (horizontal dotted lines) are given by the approximate theory.*

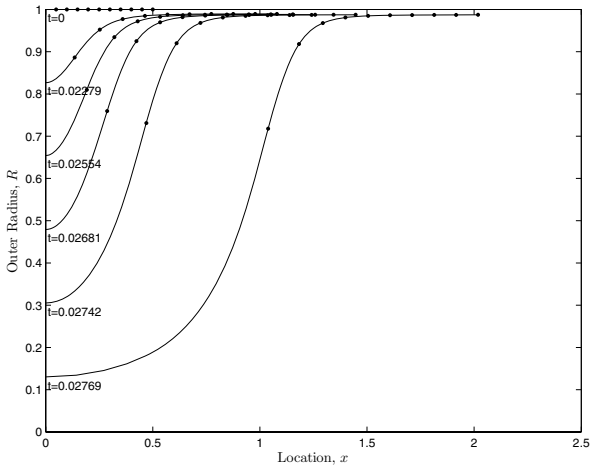

FIG. 3.10. *Outer radius of a glass tube during the evolution of the microelectrode formation under symmetric pulling with a constant force and nonuniform heating.*

the same radius in both the uniform and nonuniform cases. The only significant difference between the uniform and nonuniform cases is that uniform heating means that a larger section of the glass will be heated enough that it will significantly deform. Hence, the total extension of the glass tube before breaking is significantly longer.

3.4. Asymmetric pulling with constant force and nonuniform heating. We now consider the case of a tube that is initially located in the region $0 \leq x \leq 1$, is fixed at one end ($x = 0$), and is pulled at the other end with constant force. The tube

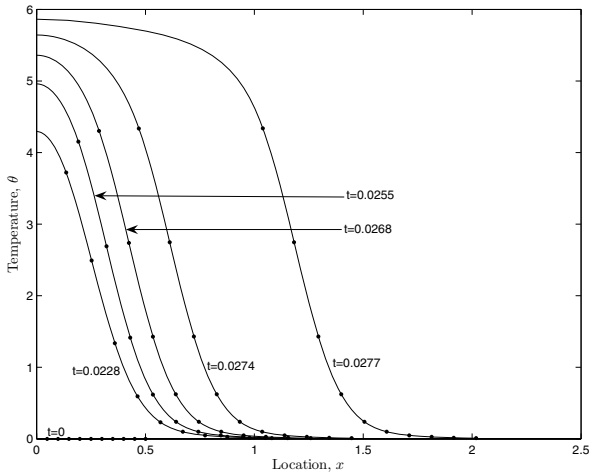

FIG. 3.11. *Temperature of a glass tube during the evolution of the microelectrode formation under symmetric pulling with a constant force and nonuniform heating.*

is heated in the same way as in the previous section, but with the maximum intensity centered on the midpoint of the tube,

$$H(x) = \exp\left(-\frac{4\pi(x-1/2)^2}{l_h^2}\right).$$

In Figure 3.9, we plotted the final shape of the electrodes at the breaking time. The dash-dot curve represents microelectrode shape of the section of the tube that remains attached to the fixed wall (reversed in x for comparison purposes), and the dashed curve represents the shape of the section to which the force was being applied. The horizontal dotted lines represent the approximate theory for the tip radius and radius far from the tip. In Figures 3.12 and 3.13, we plot the evolution of the outer radius and temperature. Again, the approximate theory gives an excellent approximation for the breaking tip radius, as explained in the above section. The difference between the electrode shapes to the left and right of the breaking point can be explained by the small differences that occur during the second stage of the evolution. Both microelectrode tips in the asymmetrical pulling case extend further than the tip for the symmetric case because the hottest part of the tube moves relative to the heater maximum. Therefore, more of the glass tube near the breaking point is significantly heated and can stretch more easily.

We note that, for spatially uniform heating, an analytical solution may be obtained using a procedure similar to that used in section 3.1. There are a number of cases to be considered, and the solutions become slightly complicated. Therefore, we present the results in Appendix B.

3.5. Variable pulling force. We now consider the case of a variable pulling force. We take a tube that is initially located in the region $0 \le x \le 1$, is fixed at one end ($x = 0$), and whose other end is attached to a mass that falls under gravity. In this case, the situation is slightly more complicated. For the vertical puller, the dimensionless stress is given by $s^{-1}(1 - F_r\ \mathrm{d}^2\ell/\mathrm{d}t^2)$. If one ignores breaking, it is easy to show that this solution will never pinch off and that $\ell \to t^2/(2F_r)$ as $t \to \infty$. This corresponds to the weight simply falling due to gravity, and the glass thread exerts a

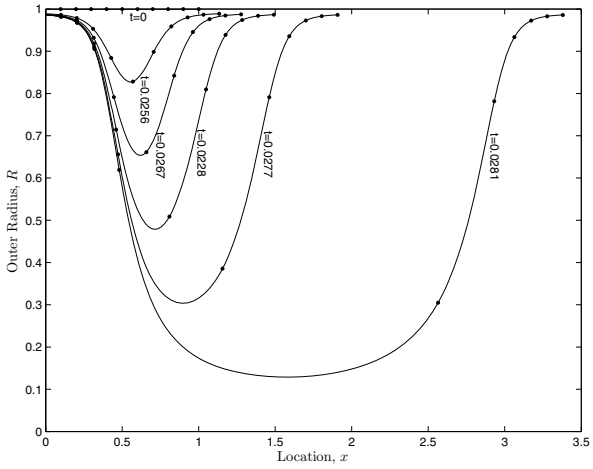

FIG. 3.12. *Outer radius of a glass tube during the evolution of the microelectrode formation under asymmetric pulling with a constant force and nonuniform heating.*

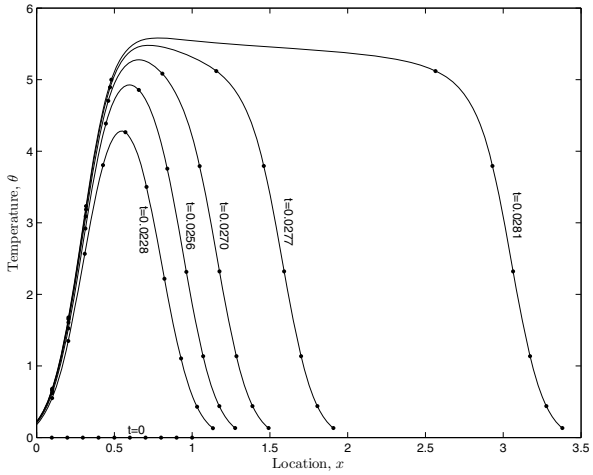

FIG. 3.13. *Temperature of a glass tube during the evolution of the microelectrode formation under asymmetric pulling with a constant force and nonuniform heating.*

negligible force on the weight. It is instructive to consider the case with no heating, i.e., the glass tube has a spatially uniform radius. In this case, it is easy to show that the stress is given by $\mathrm{d}\ln(\ell)/\mathrm{d}t$. Therefore, in the limit when $t \to \infty$, the stress tends to $2/t$, which is a decreasing function of time.

At early times, the behavior is similar to the constant force cases. This is because the initial viscosity is high and so the deformation, and hence the acceleration of the weight, are negligible. However, when the material becomes hot, it deforms rapidly. Thus, the stress increases due to thinning in the tube thickness. Therefore, the acceleration terms reduce the effective force experienced by the glass. Even though the glass is thinning, the overall stress decreases, because the force experienced by the glass is reduced by the acceleration of the weight in the same way as in the isothermal case. Therefore, we expect that the stress will attain a maximum value at finite time.

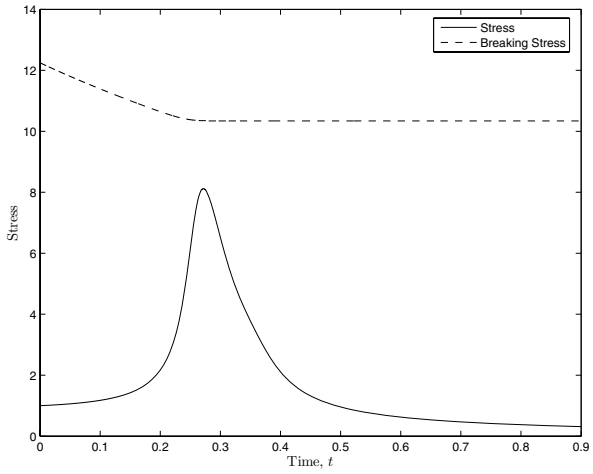

FIG. 3.14. *Dimensionless stress and dimensionless breaking stress in the glass tube closest to the location of breaking as a function of time. No breaking case.*

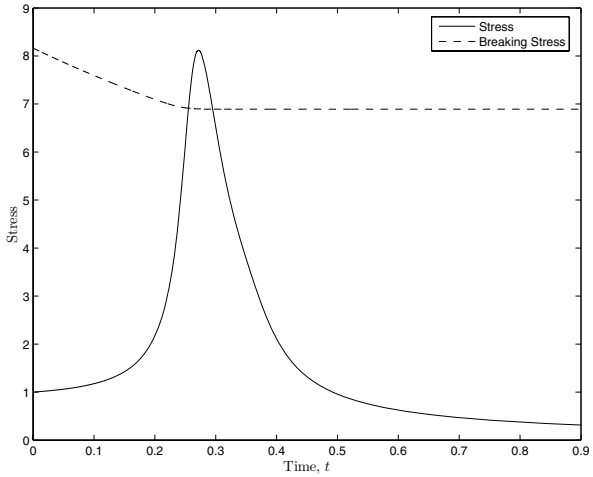

FIG. 3.15. *Dimensionless stress and dimensionless breaking stress in the glass tube closest to the location of breaking as a function of time. The tube breaks when the two curves first intersect.*

In Figures 3.14 and 3.15, we plot the dimensionless stress and the dimensionless breaking stress at the location that is closest to breaking as a function of time. For large values of $\mathcal{H}$ and C_b, as in Figure 3.14, the maximum stress is always less than the breaking stress. However, for smaller values of $\mathcal{H}$ and C_b, as in Figure 3.15, the stress may reach the breaking stress. This explains why vertical pullers typically require two pulls to break the glass tube. The first pull decreases the radius, which means that the new values of $\mathcal{H}$ and C_b for the second pull will be reduced. This implies that breaking will be more easily achieved in the second pull.

We caution that in the case when breaking does not occur, the tube becomes very thin, and inertia will ultimately become important, as shown by Stokes and Tuck [19]. Nevertheless, the inclusion of glass inertia will further reduce the viscous stress which makes it even more difficult to reach the breaking criterion. Therefore, the general

conclusion reached based on the simplified model remains useful. As we noted earlier, in this paper we focus only on successful pullings of microelectrodes, and the free-fall case will not be pursued here.

4. Discussion. We now discuss the effects of the parameters and puller designs on the shape of the final electrode. In order to do this, we will focus on the analytical solutions and results from the numerical method discussed in the previous section.

4.1. Shape control. There are two parameters that are relatively easy to vary continuously in an experimental context. These are the dimensional force, F_0, and the dimensional temperature of the heater, θ_h. In practice, one can use a graph of τ_{pinch} against $\mathcal{H}$ to choose the appropriate value of the heater strength $\mathcal{H}$ to achieve the required maximum area, $1 - \tau_{pinch}$. One then can choose C_b to give the required minimum area, s_b. Once the desired values of C_b and $\mathcal{H}$ are known, one simply chooses the dimensional force, F_0, to achieve the C_b value and then chooses θ_h to obtain the $\mathcal{H}$ value. This means that the appropriate operating conditions can be well approximated by simply using the universal graph of τ_{pinch} against $\mathcal{H}$.

While it is relatively easy to set the values of applied force and heater temperature, we also need to make sure that the glass breaks while the extension of the tube is within the physical length of the puller. This can be achieved by choosing the correct heater length, after the tip radius and other parameter values are determined. In Figure 4.1, we show how we can control the final tip radius by varying the applied force. We vary the applied force and use values of the other parameters from Tables 2.1 and 2.2. The simulation results (circles) and the approximate theory (solid line) show excellent agreement over many orders of magnitude in the applied force. By reducing the applied force, effectively, we can reduce the stress in the tube, and this allows the tube to reach a smaller radius before exceeding the breaking stress.

4.2. Sensitivity analysis. In order to determine the relative robustness of the symmetric and asymmetric methods, we performed a sensitivity analysis of the final shape with respect to changes in the parameters $\mathcal{H}$ and C_b. We found that the

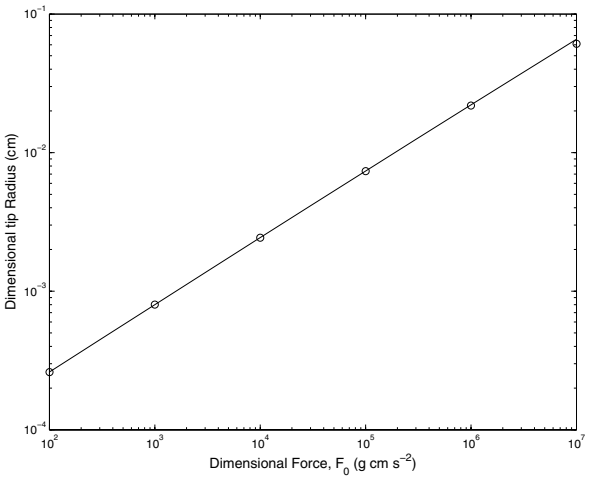

FIG. 4.1. *Dimensional tip radius as a function of the applied force.*

sensitivities are almost identical over a wide range of parameter values; therefore neither parameter has a significant advantage with regard to robustness. The symmetric puller has the advantage in that it can create two identical electrodes in a single pull. However, the asymmetric puller may be cheaper to build and easier to operate since it requires only a force be exerted at one end.

The sensitivity of vertical pullers to changes in parameters can be quite strong. This is particularly true if the glass breaks while the extension of the tube occurs near the maximum stress level. Then small increases in $\mathcal{H}$ or C_b might prevent the stress from reaching the breaking value, and no electrode would be formed. Even if this does not occur, the sensitivity of the variable force method is still substantially larger than for the constant force methods. The fact that a double pull is required also means that the procedure is much more difficult to implement and therefore less robust.

4.3. Concluding remarks. In this paper, we have simplified a model proposed in an earlier study (Huang et al., [10]) for glass microelectrode formation. Using a dimensional analysis argument, we have shown that the conductive heat transfer is small compared to the radiative and convective transfer and therefore can be neglected in the temperature equation. We have developed a Lagrangian-based method to solve the model equations and compute explicit solutions to the time-dependent equations for some simple cases. By investigating the effects of the parameters on the final shape of the microelectrodes, we have shown that vertical pullers are much less robust than horizontal pullers.

By considering the simplified models, we have been able to understand a number of important features of the resulting electrode. First, for typical parameter values, the surface tension is much smaller than the applied force, and we have shown that the ratio of the inner to outer radius will remain constant. Therefore, if a specified ratio is required in the final electrode, the only way to achieve this is to start with a tube that has that required ratio. Second, the length of the electrode tip is of the same order of magnitude as the length of the heater. This means that the tip length can be controlled by controlling the portion of the glass that is heated significantly. Third, using our approximate theory, we have shown that an excellent approximation to the tip width can be obtained from a very simple formula. This gives an extremely practical and straightforward method of determining the parameter values required to achieve a given tip radius.

In some cases, controlling the tip radius may not be sufficient, and the user may wish to control the entire tip profile. This can be achieved either by using a spatially dependent heater profile or by allowing a time-dependent pulling force. By choosing different heater profiles or pulling forces, one can produce a tip shape close to a desirable one. Since our method is simple, robust, and extremely efficient to implement numerically, it can be used to estimate the tip profile when the heating profile and/or pulling force are given. By using standard optimization techniques on this function, we then can achieve an approximation to the required profile.

Finally, the analysis and solution methodology presented in this paper are not restricted to glass microelectrode formation and may have a number of important applications in other glass formation processes. For example, the pulling of optical fibers uses a similar setup, even though the objective for optical fiber pulling is rather different. Instead of seeking the conditions to break the glass tube under stretching, a good optical fiber pulling device must ensure that the glass stretches without being broken. However, our model and numerical method can be readily applied to fiber pulling, with minor adjustments on the handling of boundary conditions.

Appendix A. Derivation of the temperature equation (2.18). In the long-wavelength limit of small radius to length aspect ratio, axial conduction can be neglected, and the heat equation is given by

$$\theta_t + u\theta_x = \frac{k}{\rho c_p}\frac{1}{y}\frac{\partial}{\partial y}\left(y\frac{\partial \theta}{\partial y}\right), \tag{A.1}$$

where y is the axisymmetric radial position and c_p and k are the specific heat capacity and the thermal conductivity of the fluid, respectively. The radiative boundary condition is given by

$$k\left.\frac{\partial \theta}{\partial y}\right|_{y=r} = 0, \tag{A.2}$$

$$-k\left.\frac{\partial \theta}{\partial y}\right|_{y=R} = \frac{k_B E_h \varepsilon_h \alpha\left(\theta_h^4 - \theta^4\right)}{1-(1-\alpha)(1-\varepsilon_h)} + \frac{k_B E_b \varepsilon_b \alpha\left(\theta_b^4 - \theta^4\right)}{1-(1-\alpha)(1-\varepsilon_b)}, \tag{A.3}$$

where k_B is the Boltzmann constant, α is the absorptivity, and θ_h is the heater temperature. We have assumed that the axial conduction is negligible and that the radiation heat exchange occurs only on the outer surface of the glass tube, as in [9].

We now nondimensionalize the heat equation (A.1) and the boundary condition (A.3) by using the scalings

$$u = u_0 u',\ \ s = s_0 s',\ \ y = R_0 y',\ \ x = \ell_0 x',\ \ t = \ell_0 u_0^{-1} t',\ \ \theta = \theta_0 + \theta_a \theta',\ \ u_0 = \frac{\ell_0 F_0}{3\mu_0 s_0}.$$

Dropping the primes, the heat equation becomes

$$Pe\left(\frac{\partial \theta}{\partial t} + u\frac{\partial \theta}{\partial x}\right) = \frac{1}{y}\frac{\partial}{\partial y}\left(y\frac{\partial \theta}{\partial y}\right), \tag{A.4}$$

where

$$Pe = \frac{\rho c_p u_0 R_0^2}{\ell_0 k} = 4.2 \times 10^{-3} \tag{A.5}$$

is the transverse Peclet number, which represents the ratio of heat advected along the thread to heat conducted across the thread. The radiative boundary condition becomes

$$\left.\frac{\partial \theta}{\partial y}\right|_{y=\frac{r}{R_0}} = 0, \qquad \left.\frac{\partial \theta}{\partial y}\right|_{y=\frac{R}{R_0}} = BiH(x,\theta), \tag{A.6}$$

where

$$Bi = \frac{\alpha k_b \theta_h^4 R_0 \epsilon_h}{k\theta_a[1-(1-\alpha)(1-\epsilon_h)]} = 3.5 \times 10^{-1} \tag{A.7}$$

is the Biot number. The dimensionless function

$$H(x,\theta) = E_h(x)\left(1 - \left(\frac{\theta_0 + \theta\theta_a}{\theta_h}\right)^4\right) + \frac{\epsilon_b[1-(1-\alpha)(1-\epsilon_h)]E_b(x)(\theta_b^4 - (\theta_0+\theta_a\theta)^4)}{\epsilon_h[1-(1-\alpha)(1-\epsilon_b)]\theta_h^4}$$

represents the magnitude of the net heat flux that is absorbed when the temperature is θ. We now assume that both Bi and Pe are small, and from (2.2) we note that

$$\mathcal{H} \equiv \frac{2Bi}{(1-\beta_0^2)Pe}. \tag{A.8}$$

We assume that the temperature has an asymptotic expansion of the form

$$\theta = \Theta_0 + Bi\Theta_1 + \cdots; \tag{A.9}$$

then substituting this into (A.4) and (A.6) and collecting the terms to zeroth and first order in Bi yields

$$\frac{1}{y}\frac{\partial}{\partial y}\left(y\frac{\partial \Theta_0}{\partial y}\right) = 0 \quad \text{with} \quad \left.\frac{\partial \Theta_0}{\partial y}\right|_{y=\frac{r}{R_0}} = 0, \quad \left.\frac{\partial \Theta_0}{\partial y}\right|_{y=\frac{R}{R_0}} = 0 \tag{A.10}$$

and

$$\frac{1}{y}\frac{\partial}{\partial y}\left(y\frac{\partial \Theta_1}{\partial y}\right) = \frac{2}{(1-\beta_0^2)\mathcal{H}}\left(\frac{\partial \Theta_0}{\partial t} + u\frac{\partial \Theta_0}{\partial x}\right) \tag{A.11}$$

with

$$\left.\frac{\partial \Theta_1}{\partial y}\right|_{y=r} = 0, \quad \left.\frac{\partial \Theta_1}{\partial y}\right|_{y=R} = H\left(x, \Theta_0\right). \tag{A.12}$$

Equation (A.10) implies that at leading order Θ_0 is independent of y. Therefore, using (A.11)–(A.12), we see that Θ_0 satisfies

$$\frac{\partial \Theta_0}{\partial t} + u\frac{\partial \Theta_0}{\partial x} = \frac{\mathcal{H}H\left(x, \Theta_0\right)}{\sqrt{s}}\sqrt{\frac{1-\beta_0^2}{1-\beta^2}}, \tag{A.13}$$

where $\beta = r/R$. For notational brevity, we use θ to denote the leading order term, Θ_0, and obtain the equation in the final form as (2.18).

At the leading order, the viscosity is independent of the radial coordinate because the viscosity is a function of the temperature.

Appendix B. Exact solution for asymmetrical pulling. In this appendix, we obtain the exact solutions for the microelectrode shape and the temperature distribution for a glass tube undergoing asymmetrical pulling with uniform heating from a finite length heater. The initial velocity at each point in the glass tube is zero, and the other initial and boundary conditions are

$$\theta(\xi,0) = 0,\ s(\xi,0) = 1,\ x(\xi,0) = \xi,\ \theta(0,\tau) = 0,\ s(0,\tau) = 1,\ x(0,\tau) = 0. \tag{B.1}$$

The heater is located between $\xi = \ell_1$ and $\xi = \ell_2$. Let τ_b be the breaking time and τ_* be the time when the material point $\xi = \ell_1$ has passed location ℓ_2.

We need to consider two different cases: $\tau_b \le \tau_*$ and $\tau_b > \tau_*$.

B.1. Case 1: $\tau_b \le \tau_*$. Let $\xi_1(\tau_b)$ and $\xi_2(\tau_b)$ be the initial locations of the material points that are at ℓ_1 and ℓ_2 at τ_b. We have $\xi_1(\tau_b) < \ell_1 < \xi_2(\tau_b) < \ell_2$. Thus, there exist five regions: (1) $0 \le \xi \le \xi_1(\tau_b)$, (2) $\xi_1(\tau_b) \le \xi \le \ell_1$, (3) $\ell_1 \le \xi \le \xi_2(\tau_b)$, (4) $\xi_2(\tau_b) \le \xi \le \ell_2$, and (5) $\ell_2 \le \xi \le 1$.

B.1.1. $0 \le \xi \le \xi_1(\tau_b)$. In this region, for $0 < \tau < \tau_b$, we have

$$\theta_\tau = 0, \quad s_\tau = -e^\theta, \quad s x_\xi = 1,$$

which, combined with (B.1), gives

$$\theta_1 = 0, \quad s_1 = 1 - \tau, \quad x_1 = \frac{\xi}{1-\tau}.$$

Thus, at τ_b, the solution is

$$\theta_1 = 0, \quad s_1 = 1 - \tau_b, \quad x_1 = \frac{\xi}{1-\tau_b}, \tag{B.2}$$

from which we obtain $\xi_1(\tau_b) = (1-\tau_b)\ell_1$.

B.1.2. $\xi_1(\tau_b) \le \xi \le \ell_1$. (I). $0 \le \tau \le \tau_1(\xi)$, where $\tau_1(\xi)$ is the time when the material point that is initially at ξ crosses the point ℓ_1. The solution is

$$\theta_2^- = 0, \quad s_2^- = 1 - \tau, \quad x_2^- = \frac{\xi - \xi_1(\tau_b)}{1-\tau} + x_1(\xi_1(\tau_b), \tau) = \frac{\xi}{1-\tau},$$

from which we obtain

$$\ell_1 = \frac{\xi}{1 - \tau_1(\xi)}$$

or

$$\tau_1(\xi) = 1 - \frac{\xi}{\ell_1}.$$

(II). $\tau_1(\xi) \le \tau \le \tau_b$. In this region, we have

$$\theta_\tau = \frac{\mathcal{H}}{\sqrt{s}}, \quad s_\tau = -e^\theta, \quad s x_\xi = 1,$$

from which we obtain

$$\begin{aligned}
&\frac{2\mathcal{H}\sqrt{1-\tau_1(\xi)}+1}{2\mathcal{H}} \ln\left[1 + 2\mathcal{H}\left(\sqrt{1-\tau_1(\xi)} - \sqrt{s_2^+}\right)\right] \\
&\quad = \sqrt{1-\tau_1(\xi)} - \sqrt{s_2^+} + \mathcal{H}[\tau - \tau_1(\xi)], \\
&\quad \left(2\mathcal{H}\sqrt{1-\tau_1(\xi)}+1\right)\theta_2^+ + 1 - e^{\theta_2^+} = 2\mathcal{H}^2[\tau - \tau_1(\xi)], \\
&x_2^+ = \ell_1 + \int_{\xi_1(\tau)}^{\xi} \frac{1}{s_2^+(\tau_1(\eta))} d\eta.
\end{aligned}$$

Therefore,

$$\frac{2\mathcal{H}\sqrt{1-\tau_1(\xi)}+1}{2\mathcal{H}} \ln\left[1 + 2\mathcal{H}\left(\sqrt{1-\tau_1(\xi)} - \sqrt{s_2^+}\right)\right] \tag{B.3}$$

$$= \sqrt{1-\tau_1(\xi)} - \sqrt{s_2^+} + \mathcal{H}[\tau_b - \tau_1(\xi)],$$

$$\left(2\mathcal{H}\sqrt{1-\tau_1(\xi)}+1\right)\theta_2^+ + 1 - e^{\theta_2^+} = 2\mathcal{H}^2[\tau_b - \tau_1(\xi)], \tag{B.4}$$

$$x_2^+ = \ell_1 + \int_{\xi_1(\tau_b)}^{\xi} \frac{1}{s_2^+(\tau_1(\eta))} d\eta. \tag{B.5}$$

B.1.3. $\ell_1 \le \xi \le \xi_2(\tau_b)$. For $0 \le \tau \le \tau_b$, we have

$$\theta_\tau = \frac{\mathcal{H}}{\sqrt{s}}, \quad s_\tau = -e^\theta, \quad s x_\xi = 1,$$

from which we have

$$\begin{aligned}
&\sqrt{s_3} - 1 + \frac{2\mathcal{H}+1}{2\mathcal{H}} \ln\left(1 + 2\mathcal{H} - 2\mathcal{H}\sqrt{s_3}\right) = \mathcal{H}\tau,\\
&(2\mathcal{H}+1)\,\theta_3 + 1 - e^{\theta_3} = 2\mathcal{H}^2\tau,\\
&x_3 = \frac{\xi - \ell_1}{s_3(\tau)} + x_2^+(\ell_1, \tau).
\end{aligned}$$

At τ_b, we have

$$\sqrt{s_3} - 1 + \frac{2\mathcal{H}+1}{2\mathcal{H}} \ln\left(1 + 2\mathcal{H} - 2\mathcal{H}\sqrt{s_3}\right) = \mathcal{H}\tau_b, \tag{B.6}$$

$$(2\mathcal{H}+1)\,\theta_3 + 1 - e^{\theta_3} = 2\mathcal{H}^2\tau_b, \tag{B.7}$$

$$x_3 = \frac{\xi - \ell_1}{s_3(\tau_b)} + x_2^+(\ell_1, \tau_b). \tag{B.8}$$

From the above equation, we determine $\xi_2(\tau_b)$ to be

$$\xi_2(\tau_b) = \ell_1 + [\ell_2 - x_2^+(\ell_1, \tau_b)] s_3(\tau_b). \tag{B.9}$$

B.1.4. $\xi_2(\tau_b) \le \xi \le \ell_2$. (I). $0 \le \tau \le \tau_2(\xi)$, where $\tau_2(\xi)$ is the time at which the material point ξ crosses the point ℓ_2. In this case, we have

$$\theta_\tau = \frac{\mathcal{H}}{\sqrt{s}}, \quad s_\tau = -e^\theta, \quad s x_\xi = 1,$$

from which we have

$$\begin{aligned}
&\sqrt{s_4^-} - 1 + \frac{2\mathcal{H}+1}{2\mathcal{H}} \ln\left(1 + 2\mathcal{H} - 2\mathcal{H}\sqrt{s_4^-}\right) = \mathcal{H}\tau,\\
&(2\mathcal{H}+1)\,\theta_4^- + 1 - e^{\theta_4^-} = 2\mathcal{H}^2\tau,\\
&x_4^- = \frac{\xi - \xi_2(\tau_b)}{s_4^-(\tau)} + x_3(\xi_2(\tau_b), \tau).
\end{aligned}$$

From the last equation, we obtain

$$\ell_2 == \frac{\xi - \xi_2(\tau_b)}{s_4^-(\tau_2(\xi))} + x_3(\xi_2(\tau_b), \tau_2(\xi)). \tag{B.10}$$

From this equation, we can find the value of $\tau_2(\xi)$.

(II). $\tau_2(\xi) \le \tau \le \tau_b$. In this case,

$$\theta_\tau = 0, \quad s_\tau = -e^\theta, \quad s x_\xi = 1,$$

from which we have

$$\begin{aligned}
&\theta_4^+(\xi, \tau) = \theta_4^+(\tau_2(\xi)) = \theta_4^-(\tau_2(\xi)),\\
&s_4^+(\xi, \tau) = \tau_2(\xi) - \tau + s_4^+(\tau_2(\xi)) = \tau_2(\xi) - \tau + s_4^-(\tau_2(\xi)),\\
&x_4^+(\xi, \tau) = \ell_2 + \int_{\xi_2(\tau)}^{\xi} \frac{1}{s_4^+(\eta, \tau)} d\eta.
\end{aligned}$$

At τ_b, we have

$$\theta_4^+(\xi,\tau_b)=\theta_4^+(\tau_2(\xi))=\theta_4^-(\tau_2(\xi)), \tag{B.11}$$

$$s_4^+(\xi,\tau_b)=\tau_2(\xi)-\tau_b+s_4^+(\tau_2(\xi))=\tau_2(\xi)-\tau_b+s_4^-(\tau_2(\xi)), \tag{B.12}$$

$$x_4^+(\xi,\tau_b)=\ell_2+\int_{\xi_2(\tau_b)}^{\xi}\frac{1}{s_4^+(\eta,\tau_b)}d\eta. \tag{B.13}$$

B.1.5. $\ell_2 \le \xi \le 1$. In this region,

$$\theta_\tau=0,\quad s_\tau=-e^\theta,\quad sx_\xi=1$$

is valid for $0\le\tau\le\tau_b$, from which we have

$$\theta_5=0,\quad s_5=1-\tau,\quad x_5=\frac{\xi-\ell_2}{1-\tau}+x_4^+(\ell_2,\tau).$$

At τ_b, we have

$$\theta_5=0,\quad s_5=1-\tau_b,\quad x_5=\frac{\xi-\ell_2}{1-\tau_b}+x_4^+(\ell_2,\tau_b). \tag{B.14}$$

B.2. Case 2: $\tau_b > \tau_*$. In this case, there are also five regions: (1) $0\le\xi\le\xi_1(\tau_b)$, (2) $\xi_1(\tau_b)\le\xi\le\xi_2(\tau_b)$, (3) $\xi_2(\tau_b)\le\xi\le\ell_1$, (4) $\ell_1\le\xi\le\ell_2$, and (5) $\ell_2\le\xi\le1$.

B.2.1. $0\le\xi\le\xi_1(\tau_b)$. In this region, for $0<\tau<\tau_b$, the solution is the same as that in Case 1,

$$\theta_1=0,\quad s_1=1-\tau,\quad x_1=\frac{\xi}{1-\tau},$$

and at τ_b the solution is

$$\theta_1=0,\quad s_1=1-\tau_b,\quad x_1=\frac{\xi}{1-\tau_b}, \tag{B.15}$$

from which we obtain $\xi_1(\tau_b)=(1-\tau_b)\ell_1$.

B.2.2. $\xi_1(\tau_b)\le\xi\le\xi_2(\tau_b)$. (I). When $0\le\tau\le\tau_1(\xi)$, the solution is

$$\theta_2^-=0,\quad s_2^-=1-\tau,\quad x_2^-=\frac{\xi-\xi_1(\tau_b)}{1-\tau}+x_1(\xi_1(\tau_b),\tau)=\frac{\xi}{1-\tau},$$

from which we obtain

$$\ell_1=\frac{\xi}{1-\tau_1(\xi)}$$

or

$$\tau_1(\xi)=1-\frac{\xi}{\ell_1}.$$

(II). When $\tau_1(\xi)\le\tau\le\tau_b$ in this region, we have

$$\theta_\tau=\frac{\mathcal{H}}{\sqrt{s}},\quad s_\tau=-e^\theta,\quad sx_\xi=1,$$

from which we obtain

$$\frac{2\mathcal{H}\sqrt{1-\tau_1(\xi)}+1}{2\mathcal{H}}\ln\left[1+2\mathcal{H}\left(\sqrt{1-\tau_1(\xi)}-\sqrt{s_2^+}\right)\right]$$
$$=\sqrt{1-\tau_1(\xi)}-\sqrt{s_2^+}+\mathcal{H}[\tau-\tau_1(\xi)],$$

$$\left(2\mathcal{H}\sqrt{1-\tau_1(\xi)}+1\right)\theta_2^+ +1-e^{\theta_2^+}=2\mathcal{H}^2[\tau-\tau_1(\xi)],$$
$$x_2^+=\ell_1+\int_{\xi_1(\tau)}^{\xi}\frac{1}{s_2^+(\tau_1(\eta))}d\eta.$$

Therefore,

$$\frac{2\mathcal{H}\sqrt{1-\tau_1(\xi)}+1}{2\mathcal{H}}\ln\left[1+2\mathcal{H}\left(\sqrt{1-\tau_1(\xi)}-\sqrt{s_2^+}\right)\right]$$
$$=\sqrt{1-\tau_1(\xi)}-\sqrt{s_2^+}+\mathcal{H}[\tau_b-\tau_1(\xi)], \tag{B.16}$$

$$\left(2\mathcal{H}\sqrt{1-\tau_1(\xi)}+1\right)\theta_2^+ +1-e^{\theta_2^+}=2\mathcal{H}^2[\tau_b-\tau_1(\xi)], \tag{B.17}$$

$$x_2^+=\ell_1+\int_{\xi_1(\tau_b)}^{\xi}\frac{1}{s_2^+(\tau_1(\eta))}d\eta. \tag{B.18}$$

The value of $\xi_2(\tau_b)$ can be obtained from the following equation:

$$\ell_2=\ell_1+\int_{\xi_1(\tau_b)}^{\xi_2(\tau_b)}\frac{1}{s_2^+(\tau_1(\eta))}d\eta. \tag{B.19}$$

This is a nonlinear equation for $\xi_2(\tau_b)$, which can be obtained using an iterative method, after replacing the integral by a numerical quadrature.

B.2.3. $\boldsymbol{\xi_2(\tau_b)\le\xi\le\ell_1}$. (I). When $0\le\tau\le\tau_1(\xi)$, the solution is

$$\theta_3^-=0,\quad s_3^-=1-\tau,\quad x_3^-=\frac{\xi}{1-\tau}.$$

(II). When $\tau_1(\xi)\le\tau\le\tau_b$ in this region, we have

$$\theta_\tau=\frac{\mathcal{H}}{\sqrt{s}},\quad s_\tau=-e^\theta,\quad sx_\xi=1,$$

from which we obtain

$$\frac{2\mathcal{H}\sqrt{1-\tau_1(\xi)}+1}{2\mathcal{H}}\ln\left[1+2\mathcal{H}\left(\sqrt{1-\tau_1(\xi)}-\sqrt{s_3^*}\right)\right]$$
$$=\sqrt{1-\tau_1(\xi)}-\sqrt{s_3^*}+\mathcal{H}[\tau-\tau_1(\xi)], \tag{B.20}$$

$$\left(2\mathcal{H}\sqrt{1-\tau_1(\xi)}+1\right)\theta_3^* +1-e^{\theta_3^*}=2\mathcal{H}^2[\tau-\tau_1(\xi)], \tag{B.21}$$

$$x_3^*=x_2^+(\xi_2(\tau_b),\tau)+\int_{\xi_2(\tau_b)}^{\xi}\frac{1}{s_3^*(\eta,\tau)}d\eta. \tag{B.22}$$

(III). When $\tau_* \le \tau \le \tau_b$ in this region, the solution is

$$\theta_3^+(\xi,\tau) = \theta_3^+(\xi,\tau_2(\xi)) = \theta_3^*(\xi,\tau_2(\xi)),$$
$$s_3^+(\xi,\tau) = s_3^+(\xi,\tau_2(\xi)) + \tau_2(\xi) - \tau = s_3^*(\xi,\tau_2(\xi)) + \tau_2(\xi) - \tau,$$
$$x_3^+(\xi,\tau) = \ell_2 + \int_{\xi_2(\tau)}^{\xi} \frac{1}{s_3^+(\eta,\tau)} d\eta,$$

where $\theta_3^*(\xi,\tau_2(\xi))$ and $s_3^*(\xi,\tau_2(\xi))$ are from (B.21) and (B.20), with τ replaced by $\tau_2(\xi)$, and $\tau_2(\xi)$ is obtained by applying (B.22) at ℓ_2:

$$\ell_2 = \ell_1 + \int_{\xi_1(\tau)}^{\xi} \frac{1}{s_3^*(\eta,\tau_2(\xi))} d\eta. \tag{B.23}$$

This is a nonlinear equation for $\tau_2(\xi)$, which can be solved using an iterative method.

At τ_b, we have

$$\theta_3^+(\xi,\tau_b) = \theta_3^+(\xi,\tau_2(\xi)) = \theta_2^*(\xi,\tau_2(\xi)), \tag{B.24}$$
$$s_3^+(\xi,\tau_b) = s_3^+(\xi,\tau_2(\xi)) + \tau_2(\xi) - \tau_b = s_2^*(\xi,\tau_2(\xi)) + \tau_2(\xi) - \tau_b, \tag{B.25}$$
$$x_3^+(\xi,\tau_b) = \ell_2 + \int_{\xi_2(\tau_b)}^{\xi} \frac{1}{s_3^+(\eta,\tau_b)} d\eta. \tag{B.26}$$

B.2.4. $\ell_1 \le \xi \le \ell_2$. (I). When $0 \le \tau \le \tau_2'(\xi)$ in this region, we have

$$\sqrt{s_4^-} - 1 + \frac{2\mathcal{H}+1}{2\mathcal{H}} \ln\left(1 + 2\mathcal{H} - 2\mathcal{H}\sqrt{s_4^-}\right) = \mathcal{H}\tau,$$
$$(2\mathcal{H}+1)\,\theta_4^- + 1 - e^{\theta_4^-} = 2\mathcal{H}^2\tau,$$
$$x_4^- = \frac{\xi - \ell_1}{s_4^-(\tau)} + x_3^*(\ell_1,\tau).$$

From the last equation, we obtain

$$\ell_2 = \frac{\xi - \ell_1}{s_4^-(\tau_2'(\xi))} + x_3^*(\ell_1,\tau_2'(\xi)). \tag{B.27}$$

From this equation, we can find the value of $\tau_2'(\xi)$, which is the time that the material point which was initially at ξ crosses ℓ_2. Note that τ_2' is different from τ_2 in region (3) since the solutions in the two regions are different.

(II). When $\tau_2'(\xi) \le \tau \le \tau_*$ in this region, we have

$$\theta_4^*(\xi,\tau) = \theta_4^*(\tau_2'(\xi)) = \theta_4^-(\tau_2'(\xi)),$$
$$s_4^*(\xi,\tau) = \tau_2'(\xi) - \tau + s_4^*(\tau_2'(\xi)) = \tau_2'(\xi) - \tau + s_4^-(\tau_2'(\xi)),$$
$$x_4^*(\xi,\tau) = \ell_2 + \int_{\xi_2(\tau)}^{\xi} \frac{1}{s_4^*(\eta,\tau)} d\eta.$$

(III). When $\tau_* \le \tau \le \tau_b$ in this region we have

$$\theta_4^+(\xi,\tau) = \theta_4^+(\tau_2'(\xi),\tau_*),$$
$$s_4^+(\xi,\tau) = \tau_* - \tau + s_4^*(\tau_2'(\xi)),$$
$$x_4^+(\xi,\tau) = x_3^+(\ell_1,\tau) + \int_{\ell_1}^{\xi} \frac{1}{s_4^+(\eta,\tau)} d\eta.$$

At τ_b, we have

$$\theta_4^+(\xi,\tau_b) = \theta_4^+(\tau_2'(\xi),\tau_*), \tag{B.28}$$

$$s_4^+(\xi,\tau_b) = \tau_* - \tau_b + s_4^*(\tau_2'(\xi)), \tag{B.29}$$

$$x_4^+(\xi,\tau_b) = x_3^+(\ell_1,\tau_b) + \int_{\ell_1}^{\xi} \frac{1}{s_4^+(\eta,\tau_b)}\,d\eta. \tag{B.30}$$

B.2.5. $\ell_2 \le \xi \le 1$. In this region we have

$$\theta_5 = 0, \quad s_5 = 1-\tau, \quad x_5 = \frac{\xi-\ell_2}{1-\tau} + x_4^*(\ell_2,\tau)$$

for $0 \le \tau \le \tau_*$ and

$$\theta_5 = 0, \quad s_5 = 1-\tau, \quad x_5 = \frac{\xi-\ell_2}{1-\tau} + x_4^+(\ell_2,\tau)$$

for $\tau_* \le \tau \le \tau_b$.

At τ_b, we have

$$\theta_5 = 0, \quad s_5 = 1-\tau_b, \quad x_5 = \frac{\xi-\ell_2}{1-\tau_b} + x_4^+(\ell_2,\tau_b). \tag{B.31}$$

Acknowledgments. We wish to thank Drs. Demetrius Papageorgiou, Michael Siegel, Yuan-Nan Young, and Wendy Zhang for useful discussions at the Focused Research Group (FRG), in Banff. Also, we thank the Banff International Research Station (BIRS) for funding the FRG, and the staff at BIRS for their wonderful efforts to make the FRG such a productive event. Finally we wish to express our gratitude to the anonymous referees who helped us to improve the paper by providing constructive comments and suggestions.

REFERENCES

[1] M. Coenen, *Festigkeit von Glasschmelzen*, Glastech. Ber., 51 (1978), pp. 17–20.
[2] Corning Glass Company, *Pyrex Glass Code* 7740*, Material Properties*, Brochure Pyrex B-87, 1987.
[3] M. M. Denn, *Continuous drawing of liquids to form fibers*, in Annu. Rev. Fluid Mech. 12, Annual Reviews, Palo Alto, CA, 1980, pp. 365–387.
[4] J. Dewynne, J. R. Ockendon, and P. Wilmott, *On a mathematical model for fiber tapering*, SIAM J. Appl. Math., 49 (1989), pp. 983–990.
[5] J. N. Dewynne, J. R. Ockendon, and P. Wilmott, *A systematic derivation of the leading-order equations for extensional flows in slender geometries*, J. Fluid Mech., 244 (1992), pp. 323–338.
[6] A. D. Fitt, K. Furusawa, T. M. Monro, and C. P. Please, *Modeling the fabrication of hollow fibers: Capillary drawing*, J. Lightwave Technol., 19 (2001), pp. 1924–1931.
[7] A. D. Fitt, K. Furusawa, T. M. Monro, and C. P. Please, *The mathematical modelling of capillary drawing for holey fiber manufacture*, J. Engrg. Math., 43 (2002), pp. 201–227.
[8] D. G. Flaming and K. T. Brown, *Micropipette puller design, Form of the heating filament and effects of filament width on tip length and diameter*, J. Neurosci. Methods, 6 (1982), pp. 91–102.
[9] P. Gospodinov and A. L. Yarin, *Drawing resonance of optical microcapillaries in non-isothermal drawing*, Int. J. Multiphase Flow, 23 (1997), pp. 967–976.
[10] G. Gupta and W. W. Schultz, *Non-isothermal flows of Newtonian slender glass fibers*, Int. J. Nonlinear Mech., 33 (1998), pp. 151–163.
[11] G. Gupta, W. W. Schultz, E. M. Arruda, and X. Lu, *Nonisothermal model of glass fiber drawing stability*, Rhoel. Acta, 35 (1996), pp. 584–596.

[12] H. Huang, R. M. Miura, W. P. Ireland, and E. Puil, *Heat-induced stretching of a glass tube under tension: Application to glass microelectrodes*, SIAM J. Appl. Math., 63 (2003), pp. 1499–1519.
[13] A. Kaye, *Convected coordinates and elongational flow*, J. Non-Newtonian Fluid Mech., 40 (1991), pp. 55–77.
[14] R. J. LeVeque, *Numerical Methods for Conservation Laws*, Birkhäuser, Boston, Cambridge, MA, 1992.
[15] S. Martinoia, P. Massobrio, M. Bove, and G. Massobrio, *Cultured neurons coupled to microelectrode arrays: Circuit models, simulations and experimental data*, IEEE Trans. Biomed. Eng., 51 (2004), pp. 859–964.
[16] A. Peskoff and R. S. Eisenberg, *Interpretation of some microelectrode measurements of electrical properties of cells*, Ann. Rev. Biomed. Eng., 2 (1973), pp. 65–80.
[17] H. Scholze, *Glass, Nature, Structure, and Properties*, (translated by M. J. Lakin), Springer-Verlag, New York, 1990, pp. 255–272.
[18] E. M. Snell, *Some electrical properties of fine tipped pipette microelectrodes*, in Glass Microelectrodes, M. Lavallee, A. F. Shanne, and N. C. Hubert, eds., Wiley, New York, 1969, pp. 111–123.
[19] Y. M. Stokes and E. O. Tuck, *The role of inertia in extensional fall of a viscous drop*, J. Fluid Mech., 498 (2004), pp. 205–225.
[20] S. D. R. Wilson, *The slow dripping of a viscous fluid*, J. Fluid Mech., 190 (1988), pp. 561–570.